



Cardiac Scaffold for Human Mesenchymal Stem Cell Facilitated Autonomous Pacing

A Major Qualifying Project submitted to the faculty of Worcester Polytechnic Institute in partial fulfillment of the requirements for the Degree of Bachelor of Science

Submitted by:

Helena Alfonzo

Syed Ali

Brian Almeida

Katie Flynn

Submitted to:

Professor Glenn Gaudette

April 30th, 2009

Abstract

HCN gene modified Human Mesenchymal Stem Cells (hMSCs) have shown the ability to restore pacemaker function in canine and murine models. However, stem cell migration from the delivery site is a major concern. To address this problem, the team designed a device to prevent migration but still allow communication between the stem cells and native cardiomyocytes. Scaffold pore size, fiber diameter and biomaterial selection were necessary to determine. The team conducted a pore size migration assay, cell deflection calculations, gap junction formation assay and cell viability assays. The results from the tests led to the design of a two part polyurethane scaffold that prevents migration of stem cells, allows gap junction formation through pores and is packaged for minimally invasive delivery.

Table of Contents

Abstract.....	2
Table of Figures	5
Table of Tables	6
Chapter 1: Introduction.....	7
Significance.....	7
Chapter 2: Literature Review	9
The Heart	9
Structure.....	9
Mechanical Function.....	12
Electrical Function	14
Arrhythmia.....	19
Artificial Pacemakers.....	20
Parts to a pacemaker	21
Types of artificial pacemakers	22
Human Mesenchymal Stem Cell (hMSC) Driven Biological Pacemaker	23
Cell Delivery.....	25
Scaffolding.....	25
Chapter 3: Project Strategy	30
Client Statement.....	30
Prioritization of Functions and Safety Measures	33
Chapter 4: Design Criteria	37
Porosity	37
Strength.....	37
Preliminary Designs.....	39
Cross-linked Scaffold.....	39
Scaffold with Pores	40
Material Analysis	41
Material Processing.....	43
Chapter 5: Design Verification	44
Culturing Mesenchymal Stem Cells	44
Experimental Design.....	45
Preparing for Cell Assays	46

Pore Size Migration Assay.....	47
Quantifying hMSC Migration.....	48
Scaffold Gap Junction Formation Assay	50
Gap Junction and Live/Dead Immunohistochemistry.....	51
Chapter 6: Experimental Results and Discussion	54
Pore Size Migration Assay – Trial 1	54
Pore Size Migration Assay – Trial 2.....	55
Cell Viability Assay	58
Gap Junction Assay Results.....	58
Migration through Polyurethane	59
Mechanical Calculations	61
Deflection of a hMSC	61
Cell Quantity Threshold.....	65
Economic, Environmental, and Ethical Impacts.....	65
Chapter 7: Final Design	67
Chapter 8: Conclusions & Future Recommendations.....	70
Appendix.....	71
Appendix A: Completed Pairwise Chart.....	71
Appendix B: Conceptual Designs	72
Appendix C: Candidate Material Analysis	73
Nitinol	73
Dacron.....	74
EPTFE.....	74
Polyurethane	75
Appendix D: hMSC Deflection Derivations.....	78
Appendix E: hMSC Deflection MatLab Syntax	80
Appendix F: Tables of all Deflection Calculations.....	86
Bibliography	88

Note: all group members contributed equally on the writing of this paper.

Table of Figures

Figure 1: Layers of the Heart Wall (Mayo Foundation).....	9
Figure 2: Chambers and Valves of the Heart (Mayo Foundation).....	10
Figure 3: Comparison of changes in LV pressure, wall thickness, and meridional stress throughout the cardiac cycle	13
Figure 4: Myocyte Action Potential (Klabunde, 2007)	14
Figure 5: Pacemaker Electric Potential (Klabunde, 2007).....	16
Figure 6: Pathway of Electrical Propagation (Oregon Health & Science University, 2008)	18
Figure 7: Normal vs. Abnormal ECG Tracings	20
Figure 8: Parts of a Pacemaker (Heartonline, 2007).....	21
Figure 9: Top Panel - Action Potential Current is Initiated Purely by Adjacent Myocytes; Bottom Panel - Adjacent Myocytes Initiating the Stem Cell's Action Potential.....	24
Figure 10: Scanning Electron Micrograph of a Scaffold (Leor et al., 2000)	26
Figure 11: Non-woven mesh of PGA fibers (METU)	27
Figure 12: Polyurethane Fibers Produced by Electrospinning	29
Figure 13: Microporous structure of polyurethane	29
Figure 14: Function Means Tree.....	32
Figure 15: Human MSCs attached to a material surface (Plopper, 2008)	38
Figure 16: Cross-linked Scaffold.....	40
Figure 17: Scaffold with Pores	40
Figure 18: Custom built wells which house the polyurethane scaffold and allow for the seeding of cells on both the upper and lower side	47
Figure 19: Preliminary Design of Stem Cell Scaffold.....	47
Figure 20: Two layers of hMSCs across a microporous polyurethane membrane	50
Figure 21: Gaudette-Pins Dual Transwell Design	51
Figure 22: Positive (left) and Negative (right) Tissue Control Slides 40x	52
Figure 23: Positive Cell Samples at 40x (left) and 20x (right)	52
Figure 24: Sample Staining of Dead (left) and Live (right) cells	53
Figure 25: Bottom of 8 μm insert (left) and bottom of well (right).....	54
Figure 26: .4 micron wells prior to scraping (left) and post scraping (right).....	57
Figure 27: 3 micron wells prior to scraping (left) and post scraping (right).....	57
Figure 28: Live/Dead Results	58
Figure 29: 3D Gap Junction Formation through Polyurethane.....	59
Figure 30: Human Mesenchymal Stem Cells on one side of the polyurethane sheet after 3 days of incubation (left); Reverse side of the same polyurethane sheet, where no cells were able to migrate to (right).....	60
Figure 31: Free Body Diagram of a hMSC.....	61
Figure 32: Moment of Inertia of a hMSC	62
Figure 33: MatLab Syntax	63
Figure 34: Deflection vs. Pore Size and Young's Modulus	64
Figure 35: Final Design Representation	67
Figure 36: BioGlue® syringe (CryoLife, 2008)	69

Table of Tables

Table 1: Pairwise Comparison Charts.....	35
Table 2: Averages and Percentages	36
Table 3: Summary of Candidate Material Properties	41
Table 4: Qualitative Material Description	42
Table 5: Material Summary	42
Table 6: Calculation Results	64

Chapter 1: Introduction

Significance

Electronic pacemakers are readily available devices that are used to solve a variety of heart problems, extending from simple heart rate and rhythm problems to complete heart failure (Rosen et al. 2004). Even though these devices are proven to be effective, they still have a variety of limitations. Among these limitations include the pacemaker's battery life, sensitivity to magnetic fields, and lead failure. These drawbacks require that a patient undergo repeated operations to replace the battery; they also inhibit the patient's ability to undergo other tests such as MRIs and CT Scans. Furthermore, there are also complications related to the implantation of the pacemaker. For instance, if the pacemaker leads are improperly placed, it can cause the wrong parts of the heart to contract, resulting in inefficient pumping and in severe cases, death (Rosen et al. 2004). Perhaps the greatest disadvantage associated with the electrical pacemaker is that it lacks the ability to provide an appropriate cardiac response when the patient is exercising or is experiencing a strong emotional reaction (Rosen et al. 2004).

Biological pacemakers are being developed as an alternative to these electrical pacemakers with the hope of mimicking the natural pacemaker and overcoming some of the electronic pacemaker's limitations. By utilizing stem cells as a biological pacemaker, they will be capable of providing an appropriate cardiac response to exercise and emotions since the cells can react to the physiological changes in the body (Rosen et al. 2004). Also, these biological pacemakers do not contain batteries or leads; therefore the device is not sensitive to magnetic fields. This would provide the patient with a better alternative to cure their heart condition.

Although stem cells have good qualities that allow them to be ideal for engineering biological pacemakers, there are some risks associated with them. One of the biggest risks is

stem cell migration. If these undifferentiated cells were to migrate to other areas of the heart, they could cause problems like fibrillation, beating of non-cardiac muscle tissue, or cancer (Rosen et al. 2004). To address this problem, the team researched a method of containing the stem cells to prevent migration while still allowing communication between the stem cells and the surrounding cardiomyocytes.

Chapter 2: Literature Review

The heart is one of the most vital organs in the human body. There are a variety of cardiac diseases and conditions that result in over 700,000 deaths per year (29% of total), making cardiac disease the leading cause of death in the United States (CDC Website, 2008).

The Heart

Structure

The heart is located just posterior of the ribcage, anatomically left of the sternum. The heart wall has three layers (see Figure 1). The outermost layer is the epicardium, which serves as a protective layer for the heart. Beneath the epicardium is the myocardium, where the bulk of the heart's mass is located; it is responsible for the majority of the contractile force when the heart beats. Lastly, the endocardium is composed of endothelial muscle cells, which are held together by connective tissue fibers called bundles (Marieb & Hoehn, 2007).

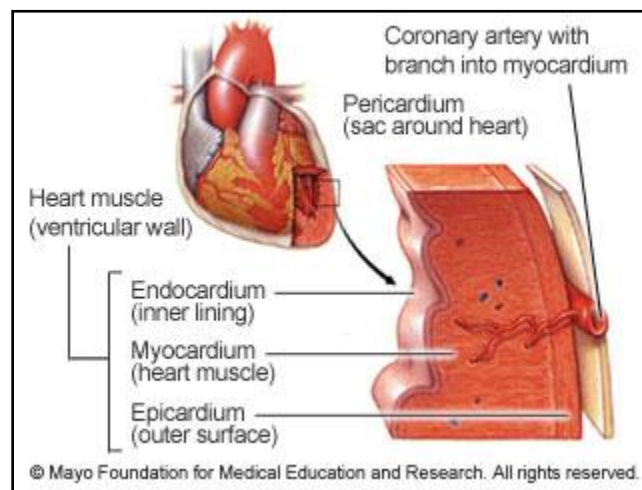


Figure 1: Layers of the Heart Wall (Mayo Foundation)

The heart is divided into four chambers and connected to several major blood vessels (see Figure 3). As deoxygenated blood enters the heart, it follows a specific path through these chambers and vessels prior to re-circulating through the body. The process begins when the vena cava empties deoxygenated blood into the right atrium. The blood then goes through the tricuspid valve into the right ventricle, where the heart contracts and pumps blood through the pulmonary valve into the pulmonary artery. This blood is then oxygenated at the lungs and brought back to the left atrium of the heart via the pulmonary veins. After a contraction, the mitral valve opens and blood empties into the left ventricle. The heart contracts again and the left ventricle pumps the newly oxygenated blood through the aortic valve into the aorta, where it circulates to the rest of the body.

The responsibility of the valves that separate the different chambers of the heart is to prevent back flow. When the heart contracts, the aortic and pulmonary valves open, while the mitral and tricuspid valves close (see Figure 2). When the heart relaxes, the opposite occurs. The cardiac cycle has two parts, which correspond to ventricular contraction and relaxation: the peak systolic pressure occurs during the heart's contraction, while diastolic pressure occurs during relaxation. Normal human blood pressure is 120 systolic pressure over 80 diastolic pressure (Fox, 2008).

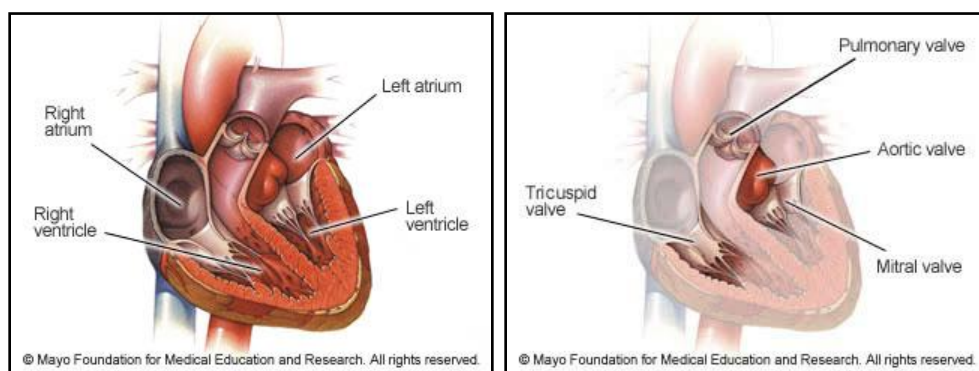


Figure 2: Chambers and Valves of the Heart (Mayo Foundation)

The heart is composed of muscle fibers which are similar to those of skeletal and smooth muscle, yet they are fundamentally different in a couple ways. Much like skeletal muscle, cardiac muscle is striated and contracts by sliding filaments. The difference, however, exists in their structure: cardiac muscle fibers are shorter, branched, and connected to each other.

On the cellular level, each cardiac muscle cell's plasma membrane is connected to other cells by an intercalated disk. Within this disk there are desmosomes, which act to hold the muscle cell together as contraction occurs (Marieb & Hoehn, 2007). In order to ensure efficient communication between adjacent cardiomyocytes, gap junctions connect the cells. These gap junctions serve as passageways for the flow of ions, which is how an electrical current gets propagated throughout the entire heart. Gap junctions are essential in the proper pacing of the heart. While various skeletal fibers have individual innervations, heart cells act together as a single unit to efficiently pump blood.

Mechanical Function

The human heart beats approximately 72 times per minute (76 to 80 for adult females; 72 for males; and 50-65 for elderly), with an average of 100,000 times per day. An average adult has about five liters circulating through their body at any moment, which equals approximately 2,000 gallons of blood being pumped by the heart every day. To put this into perspective, a seventy year old human's heart has beaten more than 2.5 billion times and has pumped more than 1 million barrels of blood (Bronzino, 2006). However, this is dependent upon a person's blood pressure, which is the force exerted by circulating blood on the walls of blood vessels. An average range of normal blood pressure is 110 to 150mmHg over 60 to 80mmHg; the higher number (peak systolic pressure) is representative of the heart as it beats and the lower number (end diastolic pressure) describes the heart as it relaxes.

An increase or decrease in blood pressure could significantly alter a person's heart condition. In a study performed by William Grossman et al., the left ventricular (LV) wall stresses were measured throughout the cardiac cycle during cardiac catheterization of thirty patients; six patients had LV pressure overload, eighteen had LV volume overload, and six patients were used as a control group since they had no evidence of heart disease. The results of this study are shown in Figure 3.

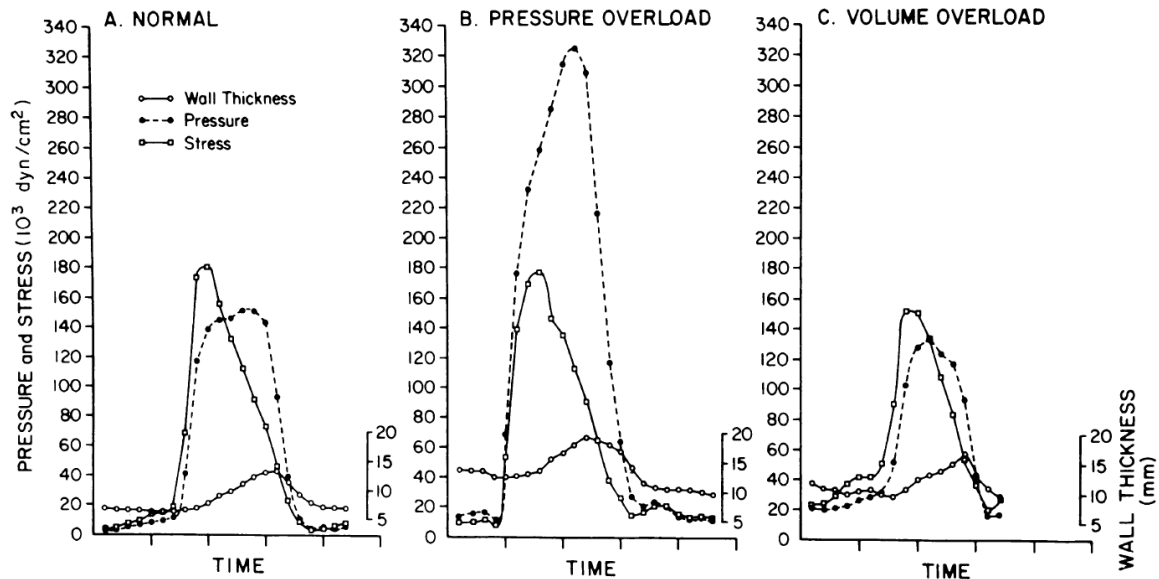


Figure 3: Comparison of changes in LV pressure, wall thickness, and meridional stress throughout the cardiac cycle (Grossman et al., 1975)

The normal peak systolic and end diastolic pressure were $117 \pm 7/10 \pm 1$ mmHg; patients with LV pressure overload had a great increase in pressure with readings of $220 \pm 6/23 \pm 3$ mmHg. Although not as significant as patients with LV pressure overload, patients with LV volume overload also showed an increase in pressure: $139 \pm 7/24 \pm 2$ mmHg. The meridional wall stress did not change dramatically between patients with no cardiac abnormalities and patients with pressure overload ($151 \pm 14/17 \pm 2 \times 10^3$ dyn/cm² compared to $161 \pm 24/23 \pm 3 \times 10^3$ dyn/cm², respectively). This was due to the fact that the pressure overload was counterbalanced by an increase in the wall thickness (1.5 ± 0.1 cm for pressure overload compared to 0.8 ± 0.1 cm for normal heart conditions). For patients with volume overload, the peak systolic meridional wall stress (175 ± 7 dyn/cm²) was slightly higher than normal heart, but was not too significant. There was a considerable increase in its end diastole wall stress, $41 \pm 3 \times 10^3$ dyn/cm² (Grossman, William et al., 1975).

Electrical Function

The heart functions with the conduction of an electrical signal through the tissue to generate a contraction. A majority of the heart's cells work just like any other muscle or nerve cell, they remain at a constant resting potential until stimulated by an outside source. These cells, which make up roughly 99% of the heart, carry out the mechanical functions the heart (Sherwood, 2004).

Figure 4 depicts the typical cardiac potential of myocytes within the ventricle. Phase 4 is the resting potential of the cardiac cell, and it remains in this state until excited by a neighboring cell. The cell maintains this negative membrane potential partly because of the i_{K1} (termed the inwardly rectifying K^+) current, which has the K^+ ions flowing outside of the cell membrane, where the concentration of K^+ ions is lower (Levy, 2007). Despite a higher concentration of Na^+ ions on the outside of the cell, the cell membrane is not very permeable to Na^+ ions. However, when the fast Na^+ channels are opened, Phase 0 occurs (Levy, 2007). Referred to as the rapid depolarization phase, this stage occurs when Na^+ channels open up, allowing a quick influx of positive Na^+ ions into the cell, causing the cell to fire an action potential (Sherwood, 2004).

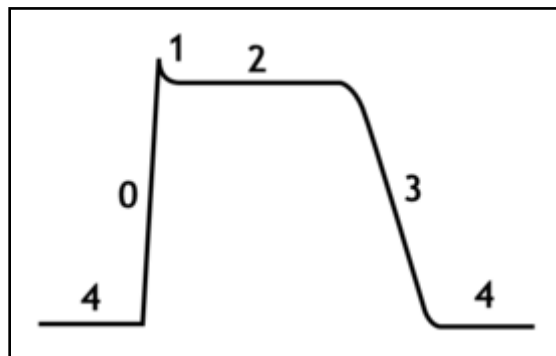


Figure 4: Myocyte Action Potential (Klabunde, 2007)

Phase 1 occurs when these Na^+ channels are all closed, and K^+ ions begin to flow outside of the cell, partially re-polarizing it (Levy, 2007). This small deflection is counteracted in Phase 2 when there is steady influx of Ca^{+2} ions, and the outflow of K^+ ions continues (Levy, 2007). Finally, the sharp decline of Phase 3 occurs when the Ca^{+2} channels close while the K^+ channels are still open (Levy, 2007). This outward current causes the cell to repolarize. The K^+ channels only close once the cell has reached its resting potential of around -80mV (Levy, 2007).

The other 1% of heart cells are unique in that they can generate and conduct their own action potentials (Sherwood, 2004). These cells, termed autorhythmic cells, are what drive the natural beating of the heart. Affected by the sympathetic and parasympathetic nervous system, these cells generate action potentials based on the how quickly blood needs to be pumped through the rest of the body (Sherwood, 2004). These autorhythmic cells also have extended refractory periods to prevent summated action potentials, which allow ample time for the chambers to empty and fill (Levy, 2007).

Autorhythmic cells do not have a resting potential like other cells; these cells slowly depolarize after an action potential has occurred and do not fire again until the threshold potential is reached (Sherwood, 2004). This behavior of repeated firing without an outside stimulus generates the natural pacemaker activity of the heart.

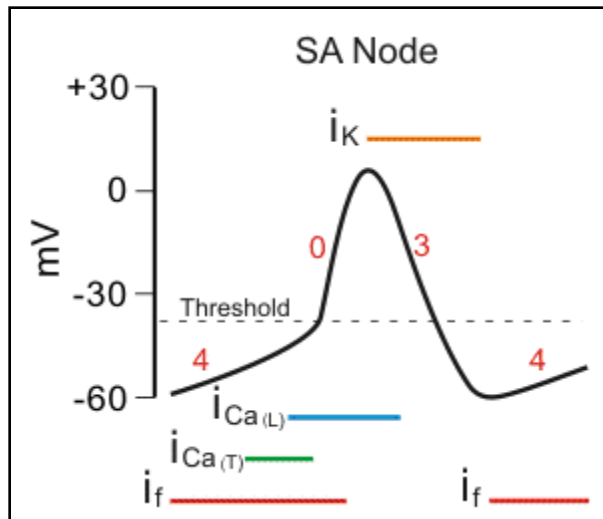


Figure 5: Pacemaker Electric Potential (Klabunde, 2007)

This autorhythmic pacemaker activity is generated by a similar controlled flow of several important ions (see Figure 5). First, the autorhythmic cells reduce the amount of K^+ ions that flow out, while constantly allowing Na^+ in (Sherwood, 2004). These paired actions slowly depolarize the cell, bringing it closer to its firing threshold (in Figure 5, this is shown by i_f). Once these actions have begun and the cell is close to reaching the threshold, voltage gated Ca^{+2} channels open; this allows an influx of ions, which raises the cell potential to the threshold (Sherwood, 2004). These Ca^{+2} channels (T-Type and L-Type) are voltage gated and only begin working once the i_f has significantly raised the potential (Levy, 2007). Once the cell has reached its threshold, the rising phase of the action potential begins (Phase 0), followed by a quick efflux of K^+ ions (Sherwood, 2004). This quick efflux of K^+ ions, which is the same inwardly rectifying K^+ current mentioned above, is shown in the above figure as i_k . This marks the cell returning to its resting potential (Phase 3).

This electrical activity happens in very specific parts of heart, which help create efficient pumping of the heart. In healthy hearts, this pacemaker activity commences at the SA node. The SA node, which is located in the right atrial wall near where the superior vena cava is connected

to the heart, is the primary pacemaker for heart function (Sherwood, 2004). The SA node is composed of two different kinds of cells: small, round cells and slender, elongated cells which initiate the current (Levy, 2007). The SA node fires an action potential roughly 70 to 80 times per minute (Sherwood, 2004). This action potential is first relayed via the four interatrial pathways at speeds of over 1 m/s to all of the contractile cells in both the right and left atrium (Levy, 2007). That signal is then propagated through the internodal pathway until it reaches the AV node, where it is delayed for roughly 100ms; this small delay allows for the blood in the atria to empty into the ventricles (Sherwood, 2004).

The AV node, often referred to as a latent pacemaker or a secondary pacemaker, is located at the base of the right atrium, alongside the dividing septum (Sherwood, 2004). The AV node is dubbed the secondary pacemaker because it only generates action potentials at a rate of 40 to 60 times per minute (Sherwood, 2004). Because it is connected via gap junctions to the SA node, which fires more quickly, the AV node must relay action potentials at the same rate to ensure efficient pumping and filling. The AV node has three different areas: AN, N, and NH zones (Levy, 2007). The AN and N regions are similar in that they both serve to help delay the propagation of the electrical signal; this helps to ensure that the atria can completely empty prior to the ventricles contracting (Levy, 2007). The NH region is the transitional area between the AV into the Bundle of His; here the action potentials transfer back from slow response (which causes the delay in the AN/N portions) to fast response (Levy, 2007).

From the AV node, the electrical signal is conducted down through the Bundle of His, which starts at the AV node and travels through the septum. In the septum, the Bundle of His breaks off into a left and right branch which travels around the base of the ventricles and up back towards the atria (see Figure 6). From here, the electrical signal is passed through the Purkinje

Fibers which wrap around the ventricles, thus completing the relay of the electrical signal (Sherwood, 2004). Much like the AV node, the Bundle of His and the Purkinje Fibers fire at a much slower rate than the SA node (around 20-40 action potentials per minute) (Sherwood, 2004). However, since the SA node is firing at a more rapid rate, both the Bundle of His and Purkinje Fibers assume the same rate as the SA node to help generate a smooth contraction. During contraction, the first part of the ventricles to contract is the myocytes near the intraventricular septum (Levy, 2007). After these cells have contracted, the signal has caused the endocardial and epicardial cells to contract (Levy, 2007). This contractile flow helps to ensure that all the blood is efficiently pushed out of the ventricles into the arteries.

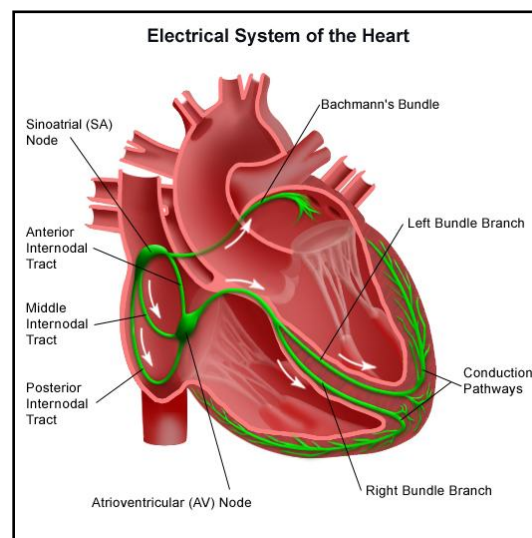


Figure 6: Pathway of Electrical Propagation (Oregon Health & Science University, 2008)

One major health issue with hearts is that the SA node can malfunction, or the connection between the SA node and AV node can become blocked. This leads to an interruption of the normal pacemaker activity. Instead of the heart beating at the rate of the SA node (about 70 times per minute), the heart is now firing at the rate of the AV node. Even though the heart is

functioning off the AV node, a slower beat results in the person feeling tired and unable to perform physical activity, along with other limitations in their natural activity.

Another potential problem with the electrical activity of the heart is when a certain group of cells becomes hyperactive. This group of cells, called an ectopic focus, fire action potentials more rapidly than the SA node (Sherwood, 2004). This can lead to irregular and premature beats of the heart, which can result in inefficient pumping of blood.

Arrhythmia

One specific form of cardiac disease is arrhythmia. Arrhythmia is clinically diagnosed when there is a loss of contractile function of the heart, which can be caused by an atrioventricular (AV) block in the Bundle of His. This results in electrical impulses traveling too fast (bradycardia), too slow (tachycardia), or erratically (fibrillation) causing the blood pressure to become altered. If the blood pressure becomes too low, the arterial blood flow does not provide for the adequate perfusion to regions of the myocardium (Katz, 1977). Figure 7 represents ECG tracings for a single cardiac cycle from a normal heart (shown on the left) and an abnormal heart (shown on the right). In a normal heart, the T wave is clearly distinct from the other waves in the ECG; also, the repolarization of the QRS wave does not go below that of the depolarization. However, in the ECG of an abnormal heart, there is no distinct T wave; instead there is a prolonged QT interval (the time between initial depolarization and final repolarization of the ventricles) and the repolarization of the ventricles goes below that of the depolarization.

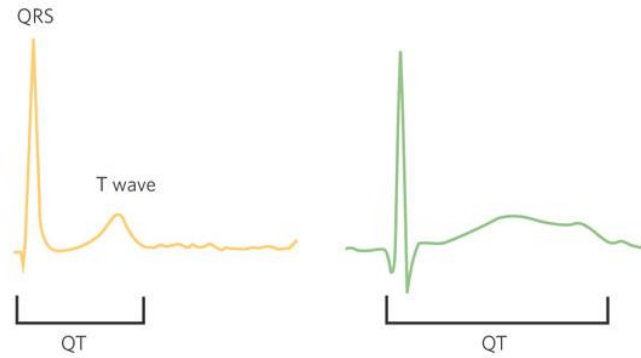


Figure 7: Normal vs. Abnormal ECG Tracings
(Sanguinette and Tristani-Firouzi, 2006)

If cardiac diseases, such as arrhythmia, are not treated, they can become life-threatening and result in cardiac arrest and sudden death. A current treatment for arrhythmia is the implantation of an artificial electrical pacemaker. These pacemakers can restore the ventricular rate when the AV block is not too severe in order to prevent death in case the AV conduction was to suddenly fail.

Artificial Pacemakers

Pacemakers can either be permanent or temporary. Temporary pacemakers are mainly used for severe cases of heart failure, such as a symptomatic bradycardia or tachycardia, or post cardiac surgery. These are used temporarily until further action, such as a surgical procedure to implant a permanent pacemaker, is taken. When the permanent pacemaker is used, it is implanted in a patient's chest. The artificial pacemaker contains one or two electrodes that come into contact with the heart's muscle fibers; the stimulating electrode is known as the cathode, and the other electrode, the anode, is placed in some distant area of the body. Pacemakers with a single electrode only stimulate the upper chambers of the heart; pacemakers with two electrodes stimulate both the upper and lower chambers of the heart. The latter pacemaker is able to be more precise in mimicking the heart rhythm (Elhendy, et al., 2008).

There are a couple of methods previously used in which the connecting wires could be brought to the heart. One method used a needle that was inserted through the chest wall into the heart, and then the electrodes were threaded through the needle. Another method used was stitching the wires into the heart muscle. The most recent method is to have the electrodes pass through the veins via a catheter and into the chambers of the heart so that there is contact with the inner surface of the right ventricle (Elhendy, et al., 2008).

Parts to a pacemaker

There are three distinct parts to a pacemaker: a generator, leads, and electrodes (see Figure 8).

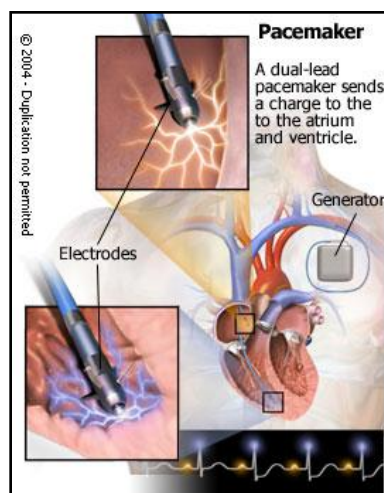


Figure 8: Parts of a Pacemaker (Heartonline, 2007)

The generator, which is responsible for generating the electric impulses that correct the irregular heartbeat, is a small box that is on average 2 inches wide and weighs approximately 3 ounces; however, they can be slightly larger or smaller. This part of the pacemaker is battery-powered, and most use lithium batteries that last for 5 to 10 years. After the battery runs out, the entire generator has to be replaced. Extruding from the generator are the leads that are typically composed of platinum and have an insulating coating of silicone or polyurethane. The leads'

function is to carry the electrical impulses from the generator to the electrodes, which are located at the tip of each lead. The purpose of the electrodes is to deliver the necessary electrical impulses to the heart.

Types of artificial pacemakers

A major concern for using artificial pacemakers is that the heart's normal impulse is disturbed and offset by the artificial pacemaker, especially during the apex of the T wave. If this ensues, ventricular fibrillation will most likely occur. As a consequence, the "synchronous pacemaker" is most often used. This type of pacemaker is able to sense the atrial excitation wave, have an appropriate delay (approximately equal to a normal PR interval), and then stimulate the ventricles.

The "standby pacemaker" is also often used because it can turn itself off when the heart does not need it. This pacemaker can sense the ventricular R wave when it occurs faster than the built-in, fixed rate of the pacemaker or when the R wave signals the pacemaker to fire without delay. In the former case, the pacemaker will block the next electrical stimulus; in the latter case, the electrical stimulus follows the refractory period of the R wave.

The most recent artificial pacemakers are externally programmable, which allows the cardiologist to be able to select specific pacing modes for individual patients. Some of these pacemakers have multiple electrodes that stimulate different areas of the heart to maintain the heart's normal pulse. Another recent pacemaker used is the biventricular pacemaker: a triple-lead pacemaker that simultaneously stimulates both ventricles of the heart in addition to pacing the right atrium. Most of these recent pacemakers incorporate a built-in device that shocks the heart back into a normal rhythm if it were to stop or if there was a serious rhythm abnormality. If a pacemaker uses this feature, it was called an implantable cardioverter defibrillator.

Human Mesenchymal Stem Cell (hMSC) Driven Biological Pacemaker

In order to overcome the mentioned limitations of artificial pacemakers, the possibility of using biological pacemakers is being explored. Within these biological pacemakers are mesenchymal stem cells, which are multipotent stem cells that have the ability to differentiate into multiple cell lines like muscle, bone, cartilage, and tendon cells. Although these cells are available in different parts of the body, the most common place where these cells are obtained from is bone marrow (Rosen et al., 2004). This cell's ability to differentiate into multiple cell lines makes it attractive for different kinds of cell therapies. Another advantage of mesenchymal stem cells is that they can be extracted from the patient's own bone marrow, so therapies involving hMSCs will be autologous, reducing the risk of an immune response (Rosen et al., 2004).

Researchers are studying adult mesenchymal stem cells as a possibility for providing an off the shelf cell therapy because of the body's low immune reaction to the stem cells. This is referred to as allogeneic stem cell transplantation. Due to the cells' ability to transfer dye and to transmit current to other cells (not only within the same cell line, but also to other cell lines like cardiomyocytes), scientists are also researching the possibility of using adult mesenchymal stem cells as a vessel to deliver genes as well as small molecules (Rosen et al., 2004).

After acknowledging these potential uses for adult mesenchymal stem cells, Rosen and his colleagues decided to explore the cells' gene therapy possibilities and take it one step further. Their idea was to create a biological pacemaker by using adult mesenchymal stem cells that had been modified with the appropriate genes.

In a normal pacemaker cell, the cell's own depolarization initiates an action potential in the cell. This action potential is then transmitted to other cells via gap junctions, passing down

the current. For adult mesenchymal stem cells to mimic this natural depolarization, the cells would have to be modified in order to express an HCN isoform (Rosen et al., 2004). The HCN (Hyperpolarization-activated cyclic nucleotide gated) channels open in response to depolarization after an action potential. The opening of these channels allows an influx of sodium ions which is the cause of the spontaneous repolarization seen in Figure 5. The sodium ions then flow to the adjacent myocytes through gap junctions as seen in Figure 9. This occurs until threshold for the myocyte action potential is reached. The action potential is propagated to other myocytes through the gap junction chain. This mechanism allows for the synchronization of the depolarization current to the diastolic current, creating an on/off switch for the current to fire (Rosen et al., 2004). In this case, both the stem cell and the adjacent cardiomyocyte would work as a pacemaker. The advantage of this method is that this approach does not need the stem cell to differentiate into a pacemaker cell in order to perform its function.

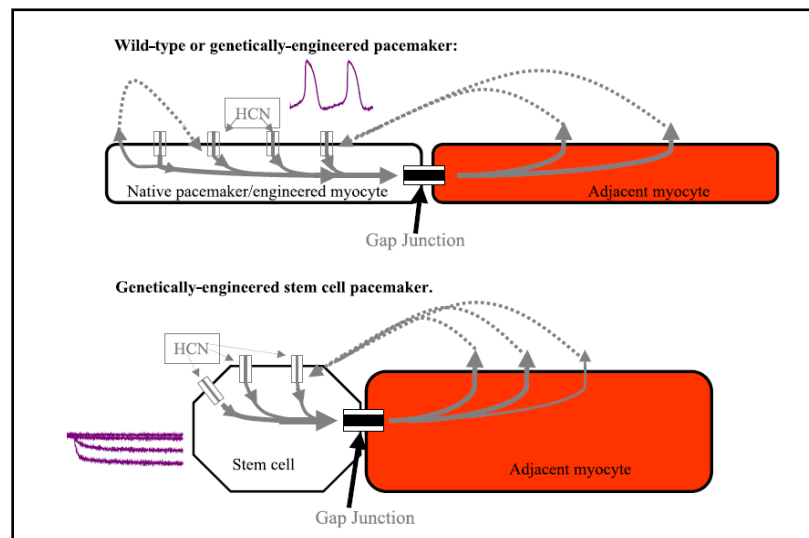


Figure 9: Top Panel - Action Potential Current is Initiated Purely by Adjacent Myocytes; Bottom Panel - Adjacent Myocytes Initiating the Stem Cell's Action Potential

Although adult mesenchymal stem cells offer a great advantage to the field of medicine by providing the possibility of biological pacemakers, there are still some great concerns that need to be addressed before this process becomes viable. Concerns include duration of function

of the biological pacemaker in comparison to the electronic pacemaker, immunological response from the body leading to cell rejection, neoplasia, cancer, migration of the cells from the implanted site to other areas of the heart or the rest of the body, and stem cell differentiation into other types of cells (Rosen et al., 2004).

Cell Delivery

Discussions with Professor Glenn Gaudette (Worcester Polytechnic Institute) in 2008 yielded certain possibilities for delivering the modified hMSCs to the heart. One method discussed was an intravenous vector. This vector had limited transfection efficiency and little to no targeted delivery (Gaudette, 2008). Another method discussed was direct injection into the heart wall. While direct, this method's limitations include blowback of delivery serum and little control over cell migration (Gaudette, 2008).

Scaffolding

If dissociated cells were to be injected into the body it would be nearly impossible to control the shape, size, and location of the implanted cells (Shimizu et al., 2002). In order to help control these factors, scientists use different types of scaffolds. These scaffolds work as a support frame for cells to attach to and grow (see Figure 10). In order to keep the cells alive, the scaffold must permit the diffusion of cell nutrients and other molecules important for proper cell function. In the case of an implant, the scaffolds can be used to not only deliver cells, but biochemical factors as well. Another advantage of scaffolds is their ability to manipulate cell behavior by applying a series of mechanical and biological stresses. The biggest challenge posed by the use of scaffolds is the lack of cell migration into the 3-D structure. This is a problem because in healthy

myocardial tissue, cells are considerably dense when compared to other tissue including cartilage and vascular tissue (Shimizu et al., 2002).

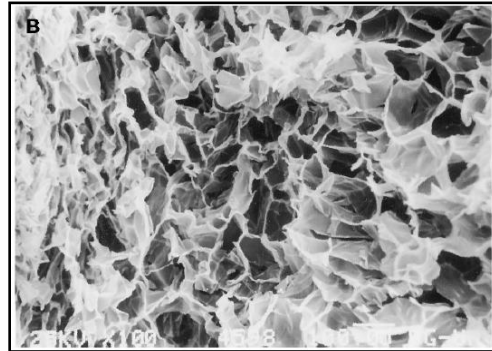


Figure 10: Scanning Electron Micrograph of a Scaffold (Leor et al., 2000)

Different materials can be used to create these scaffolds depending on the mechanical conditions having to be withstood. The main materials used for scaffolds containing cardiac cells can be synthetic or biological. Among the synthetics it is possible to find woven nylon (PET – also known as Dacron), polytetrafluoroethylene (ePTFE), poly(glycolic acid) (PGA), gelatin and alginate (Shimizu et al., 2002). On the other hand, biological materials like gluteraldehyde-cross-linked biological membranes, bovine tissue, and collagen scaffolds are also used (Robinson et al., 2005).

There are several different ways of synthesizing tissue engineering scaffolds. One process is nanofiber self-assembly. The main advantage of this method is that the biomaterials created with this method develop properties similar to those of natural extracellular matrix (ECM). This similarity allows the scaffold to be more biocompatible than other scaffolds, including those derived from animal tissue. (Ma et al, 2005)

Another way that these scaffolds can be synthesized is by using textile technologies. This process is used when non-woven meshes of different polymers are desired (see Figure 11). These

have been used successfully in growing different types of cells. The drawback of this method is that it is hard to control pore size and level of porosity. (Ma et al, 2005)

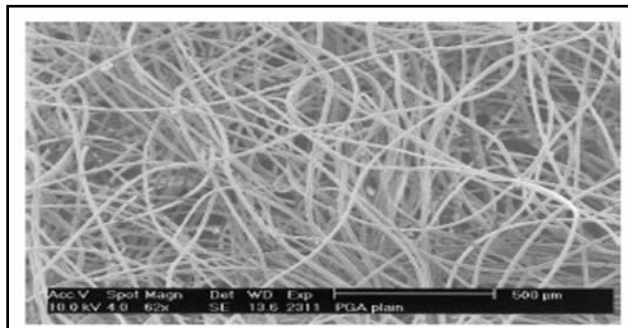


Figure 11: Non-woven mesh of PGA fibers (METU)

Solvent casting and particulate leaching is an additional way of synthesizing scaffolds. This method allows tissue engineers to control the porosity of the scaffold providing a material with a regular pore pattern. The drawback is that there is a limit on how thick the scaffold can be. Solvent casting starts by mixing the desired polymer into an appropriate organic solution. The solution is then poured into a mold and some porogens are added to the mix. Porogens are particles like sodium chloride, saccharose, or gelatin that are added to the solution before it sets. When these particles are removed they will give the scaffold its desired porous properties, including the size and amount of pores found in the scaffold. Once the polymer has been casted, the solution is allowed to evaporate leaving the polymer scaffold with the porogens still embedded in it. In order to remove the porogens, the scaffold is submerged in a liquid that dissolves the particles. Another drawback of this process is if all the porogens are not completely removed from the material, then these particles can damage the cells that are implanted onto the scaffold (Ma, 2005).

Scientists have tried to overcome the drawbacks of the solvent casting and particulate leaching process by creating new means of making these 3-D structures. To avoid the damage

caused by the porogens that were not properly dissolved, they have moved from solid porogens to gas porogens. This process called gas foaming starts by creating a disc shaped mold out of the preferred polymer by means of compression molding with heat. In order to make the material porous, the disc is placed into a chamber where CO₂ at high pressures is pumped in. The discs remain inside for a couple of days and then the chamber is slowly decompressed back to atmospheric pressure. During their time in the chamber, the discs are allowed to absorb the CO₂ which create the desired porous 3-D matrix. Once all the CO₂ is removed, the structure maintains its shape. Although this process solves the problem caused by not fully dissolved porogens, it still has some disadvantages. The main drawback of this process is that the heat used during the compression molding part of the scaffold formation limits the materials that can be utilized (Ma, 2005).

Another method of creating scaffolds is electrospinning, which uses high voltages in combination with distance from the material source to the base in order to produce a cross-linked mesh. It can produce polymer fibers of nanometer to micrometer size in diameter; Figure 12 shows 1.0µm polyurethane fibers that were produced via electrospinning. In a study performed by Angelo Pedicini et al., the authors electrospun the polyurethane solution from a 1mL glass pipette with a capillary tip of approximately 1 mm inner diameter. A stainless steel electrode was placed in the polymer solution. These were then spun onto a grounded aluminum foil sheet (Angelo Pedicini et al., 2003).

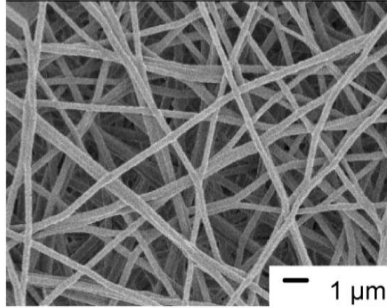


Figure 12: Polyurethane Fibers Produced by Electrospinning
(Angelo Pedicini et al., 2003)

A possible method for producing a biomaterial with pores is one that was done by Ze Zhang et al. in their study. The authors prepared a 7% (w/v) polyurethane solution by dissolving polyurethane pellets in 1,4-dioxane. They used phase inversion and freeze-drying to prepare the polyurethane tubes in an external cooling fashion. A glass capillary was inserted into a glass tube to form a casting mold, and then the polyurethane solution was poured into the space between the two glass tubes. Various cooling treatments were used for the polyurethane solution to become a solid; pore size is dependent upon the cooling rate. To remove the solvent, the mold was freeze-dried. Once the polyurethane was removed, it was sterilized in 70% alcohol (Zhang et.al., 2003). Figure 13 shows the microporous structure of polyurethane by using this methodology.

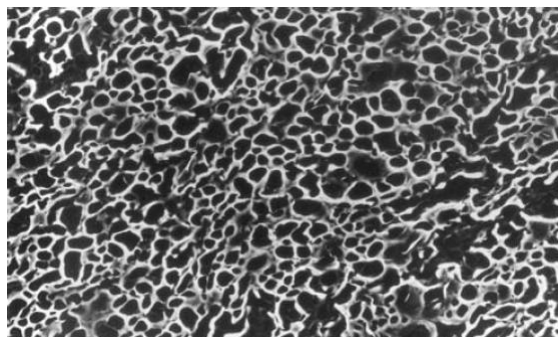


Figure 13: Microporous structure of polyurethane
(Zhang et al., 2003)

Chapter 3: Project Strategy

Client Statement

The goal of this project is to design a scaffold that will hold stem cells which are to be used as a biological pacemaker for implantation into the heart. The scaffold, which will be implanted within the ventricular septum via a minimally invasive approach, will immobilize the cells and prevent them from spreading to other areas of the heart or body. The scaffold will contain pores large enough to allow the stem cells to form gap junctions with neighboring myocytes, but small enough that they keep the stem cells within the container. This design will not impede the formation of these gap junctions, which are necessary to propagate an electrical current through the heart. The scaffold should be permanent and durable enough to withstand the normal contractile forces that are associated with heart function. The scaffold will be placed adjacent to living cardiomyocytes, and therefore, should not impede the normal physiological functions of these cells.

Functions

- Immobilize cells – scaffold inhibits cells from migrating away from designated target location (i.e. physical barrier, chemical treatment, etc.)
- Allow/facilitate formation of gap junctions, which are essential for the propagation of an electrical signal
- Ability to be implanted into the ventricular septum
- Interacts with the heart's normal function – scaffold can withstand contractile forces of the heart
- Support malfunctioning or damaged areas of the heart by allowing cells to pace the heart
- Scaffold does not interfere with normal physiological functions
- Scaffold should be permanent
- Scaffold should be placed within close proximity of living myocytes
- Scaffold does not impede electrical activity of the cells

Specifications

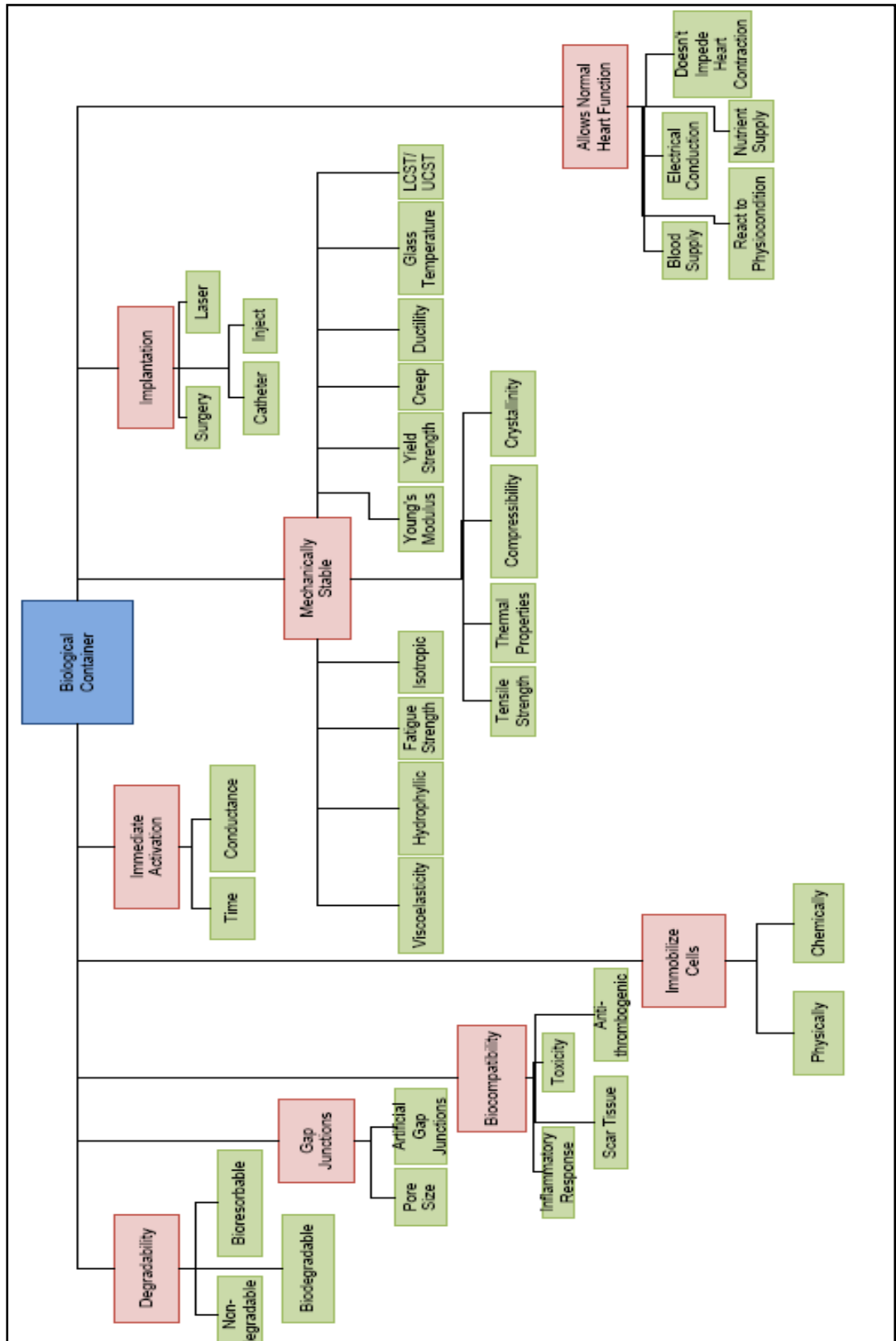
- Cells cannot pass through the mesh (pore size will be less than 3 micrometers)
- Cells must contact myocytes to allow gap junction formation
- Gap junctions should be able to form within 48 hours

Constraints

- Safety - scaffold should not degrade or break free
- Scaffold should be biologically inert and biocompatible
- Scar tissue formation should not impede gap junction formation
- Size – should not drastically impede the normal mechanical function of the heart, necessary length to seed 700k cells
- Scaffold should be implanted by means of minimally invasive surgery
- Time – the project needs to be completed by April 30, 2009
- Cost – the total cost of the project should not exceed \$624

After the functions of the device were identified, a functions means tree, shown in Figure 14, was constructed. The functions means tree allowed the team to visualize the scaffold's functions and the possible approaches to attaining those functions.

Figure 14: Function Means Tree



Prioritization of Functions and Safety Measures

Pairwise comparison charts were used during the engineering design process in order to identify which features of the design are most important (see Table 1). The two functions that the pairwise comparison charts analyzed were safety and first degree functions (degradability, biocompatibility, etc.) These two charts helped to prioritize what functions the group should be more concerned with when designing the cardiac scaffold.

The first degree functions are defined as:

- Degradability: the ability of the material to break down in a controlled manner and be absorbed by the body
- Biocompatibility: the material causes little to no immune response (this includes minimizing the formation of scar tissue around the scaffold)
- Immobilization: keeping the cells inside the scaffold rather than have them migrate around the heart or other areas of the body
- Allow gap junction formation: gap junctions form in order to communicate with cardiomyocytes allowing it to pace the heart
- Myocardium attachment: it will attach to the heart (either inside of the heart wall or just placed on the wall surface)
- Mechanically stable: the material will not break down or deform due to the mechanical forces experienced when implanted in the heart.

The safety functions are defined as:

- Inflammatory: seriousness of inflammatory response to the implant in the heart
- Thrombogenesis: risk of formation of blood clots

- Scar tissue: threat of scar tissue formation around the implanted material
- Cell proliferation: stem cells dividing and growing inside of the scaffold
- Migration: danger of stem cells migrating out of the scaffold
- Toxicity: risks of having a toxic material in the heart
- Implant complications: how important is it to keep in mind possible complications?
Would a fail-safe mechanism be important to have?
- Compliance mismatch: risks of mechanical mismatch between the implanted material and the heart (the material being either too soft or too hard)
- Scaffold breaking free: dangers of scaffold breaking free, effects in the patient
- Removability: importance of the scaffold's ability to be removed after implantation in the event of any complication
- Ease of implantation: importance of the material-user (doctor) interface in the moment of implanting the device
- Integration: importance of the material being integrated by the body (cells interacting with the implant)
- pH Balance: since implants can affect the pH balance of the surrounding area, evaluate the importance of controlling pH balance

The two pairwise comparison charts were sent to and filled out by Professor Glenn Gaudette, Jacques Guyette, Joseph Dell'Orfano, MD, and Ira S. Cohen M.D., Ph.D. The chart is filled by writing either "0" (for not important) or "1" (for important) in the white boxes depending on the level of importance of the function being evaluated. The main function that is being rated is located horizontally while the vertical functions are the ones used for comparison.

For example, if degradability was more important than biocompatibility then the corresponding box would be filled in with a number “1”; but if immobilization was more important than degradability then a “0” would be written for that box.

Table 1: Pairwise Comparison Charts

PWCC Safety functions	Inflammatory	Thrombogenesis	Scar tissue	Cell proliferation	Migration	Toxicity	Implant complications	Biomechanical mismatch	Bag breaking free	Removability	Ease of implantation	Integration	pH balance	Total
Inflammatory	█													
Thrombogenesis		█												
Scar tissue			█											
Cell proliferation				█										
Migration					█									
Toxicity						█								
Implant complication							█							
Bio- mechanical mismatch								█						
Bag breaking free									█					
Removability										█				
Ease of implantation											█			
Integration												█		
pH balance													█	

PWCC 1st degree functions	Degradability	Biocompatibility	Immobilization	Allow Gap Junction formation	Myocardium attachment	Mechanically stable	Total
Degradability	█						
Biocompatibility		█					
Immobilization			█				
Allow gap junction formation				█			
Myocardium attachment					█		
Mechanically stable						█	
Total							

Table 2 shows the final percentages in order from highest to lowest with their corresponding function. To calculate the percentage of importance for each function, the

averages were first taken for each row from each respondent. For example, if the four totals for degradability were 2, 3, 2, and 0, the average would be:

$$\frac{2 + 3 + 2 + 0}{4} = 1.75$$

Biocompatibility should be the main priority and focus for first degree functions, followed by gap junction formation, myocardium attachment, mechanically stable, immobilization, and lastly, degradability. When designing the scaffold for safety, the concern with the scaffold breaking free is of greatest importance, followed by integration, toxicity, thrombogenesis, implant complications, scar tissue, migration, ease of implantation, inflammation, biomechanical mismatch, pH balance, cell proliferation, and removability.

Table 2: Averages and Percentages

PWCC Safety functions	Average	Percentage (%)
Bag breaking free	10.25	13.14
Integration	8.5	10.90
Toxicity	8.25	10.58
Thrombogenesis	8	10.26
Implant complication	7.25	9.29
Scar tissue	6.5	8.33
Migration	6.5	8.33
Ease of implantation	5.5	7.05
Inflammatory	4	5.13
Bio- mechanical mismatch	4	5.13
pH balance	3.5	4.49
Cell proliferation	3	3.85
Removability	2.75	3.53
Total	78	100

PWCC 1st degree functions	Average	Percentage (%)
Biocompatibility	4.5	30.0
Gap junction formation	4.25	28.33
Myocardium attachment	2.5	16.67
Mechanically stable	2	13.33
Immobilization	1.75	11.67
Degradability	0	0
Total	15	100

Chapter 4: Design Criteria

Porosity

In order to contain MSCs and allow the formation of gap junctions, the scaffold material must be porous. Pore size is critical; it must be large enough to allow for the passage of electrical signals yet not too large to permit leakage of stem cells (Rosen et al, 2004). Other factors beyond the diameter of the pore must be considered as well. When a biomaterial is subjected to compressive stress, the average size of the pores will decrease and thus the permeability of the material will lessen (O'Brien et al 2007). A study by O'Brien et al. concerning the porosity of a scaffold and its effects on stem cells showed that with increased pore size and permeability, greater levels of metabolic diffusion occur and consequently induce stem cell proliferation (O'Brien et al 2007).

Too much porosity yields a negative effect that must be avoided in the design of a scaffold in the heart. Both of the studies verify the importance of selecting a critical pore size to achieve the desired functions, and based on their experimental results and the known properties of MSCs, an optimal pore size will likely be between 0.5-10 μ m.

Strength

The scaffold must be strong enough to withstand the contractile/relaxation motion of the heart, yet flexible and adaptable to allow mesenchymal stem cells to proliferate. The strength of heart contraction and relaxation is measured through blood pressure. The systolic measurement is the force at which the heart contracts to pump blood into the arteries and to the rest of the body. A healthy heart should not pump blood at a greater pressure than 120mmHg. The diastolic

pressure is the force at which the arteries relax. A healthy heart should yield a diastolic pressure of approximately 80mmHg (American Heart Association, 2008). A scaffold material subjected to the systolic and diastolic pressure must withstand forces higher than 120/80mmHg respectively, to ensure that it will not break under repeated contractile and relaxation forces.

The scaffold material must also be flexible to allow mesenchymal stem cell proliferation and ease implantation. The stem cells must be able to proliferate within the scaffold to ensure that as old cells die, new ones are generated to facilitate the communication with cardiac myocytes. Over-proliferation is not a concern in the design of the scaffold as MSCs are attachment dependent: they will adhere to the inner wall of the scaffold and will not be concentrated in the center. As a result, this cell distribution will not impose any mechanical stress on the scaffold that could potentially cause it to burst. Figure 15 shows a distribution of MSCs as they would appear adhered to a surface.

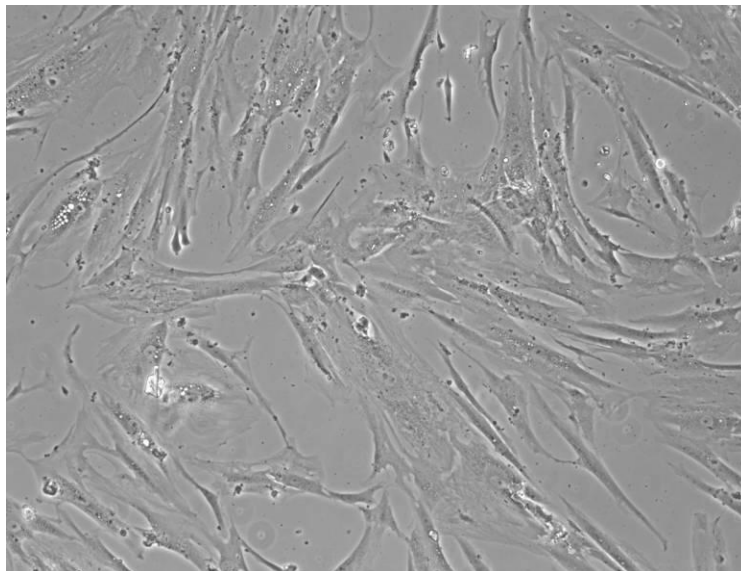


Figure 15: Human MSCs attached to a material surface (Plopper, 2008)

Lastly, the material must be simple to implant into the ventricular septum through the use of a catheter. This minimally invasive approach will require a flexible and injectable material to effectively be inserted.

Preliminary Designs

The design team drafted various conceptual designs which are located in Appendix B. Based on those early ideas the team prepared two preliminary designs. One is a fibrous cross-linked scaffold and the second a hollow scaffold with pores. Both will be in the shape of a football, with the inside being hollow to allow cells to be held inside. Both designs look to maximize the surface area with which the modified hMSCs could form gap junctions with cardiac myocytes. The main difference between the designs depends on the manufacturing technique: the cross-linked scaffold will need to be electrospun while the alternative design will utilize solvent casting or particulate leaching.

Cross-linked Scaffold

One conceptual design is a cross-linked scaffold. For this design, the fibers of the biomaterial will be interwoven via electrospinning (see Figure 16; note: the diagram is not scaled to size). For this design the material would first be electrospun into the football shape; this shape allows for a maximized surface area for the cells to attach to in order to form gap junctions. The cells would then be injected through the ends of the scaffold. A concern with this design, however, is closing off the ends once the cells have been injected. If the ends were to be left open, an infection could occur. This would result in the patient needing to go through an additional surgery to remove the infection from the heart before further complications resulted.

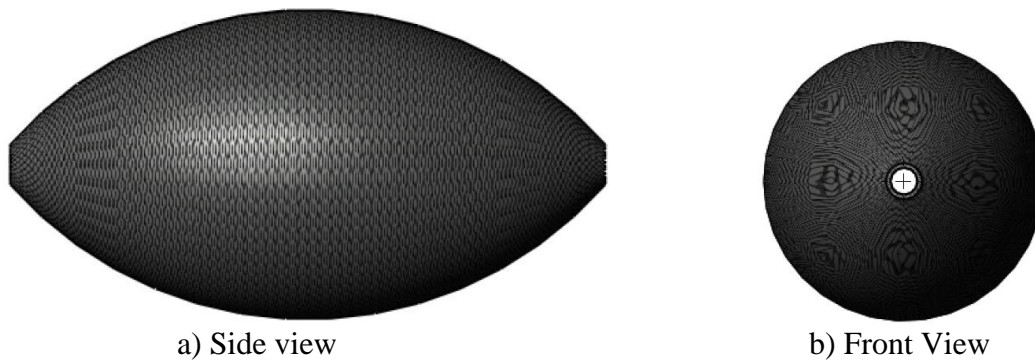


Figure 16: Cross-linked Scaffold

Scaffold with Pores

The second conceptual design is a scaffold that contains a hollow interior with scattered pores located on all sides of the exterior (see Figure 17; note: the diagram is not scaled to size). The hMSCs will be placed on the inside of this scaffold, allowing for gap junction formation through the pores. One advantage this design has over the electrospun design is that the pore size can be more controlled and concise since it will be produced using solvent casting or particulate leaching. A major disadvantage of this design, similar to that of the electrospun scaffold, is the empty space where the cells will be located, allowing for the potential for bacteria to grow and produce an infection. Another disadvantage of this design is that there will be fewer pores than the electrospun scaffold for the cells to form gap junctions with.

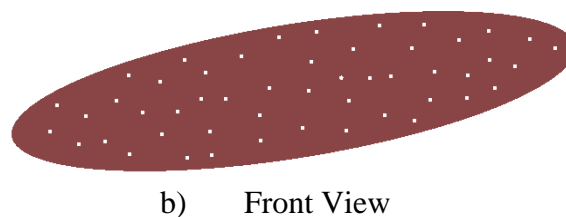
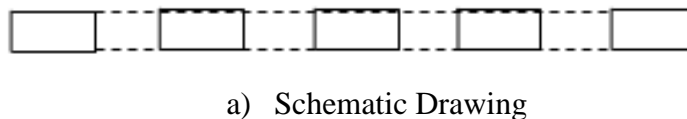


Figure 17: Scaffold with Pores

Material Analysis

In order to appropriately choose a material capable of withstanding the mechanical stresses of the heart, preventing human mesenchymal stem cell migration and other complications, common materials being employed in cardiovascular applications were evaluated. The three most common materials utilized for the production of synthetic vascular grafts are Polyethylene Terephthalate (PET) also known in the medical industry as Dacron, Polytetrafluoroethylene (PTFE), and Polyurethane (InspiredMD Corporation, 2005). In addition, Nitinol is a main component of the vascular stent business due to its particular properties. Table 3 summarizes the team’s findings regarding material properties. A summary of the materials’ characteristics under each condition evaluated can be found in Table 4.

Table 3: Summary of Candidate Material Properties

	Nitinol	Dacron (PET)	ePTFE	Polyurethane (ChronoFlex® C)
Biocompatible	Yes	Yes	Yes	Yes
Cytotoxic	no	no	no	no
Elastic Modulus	1160-1200 *10 ⁴ psi	40-60*10 ⁴ psi	5.8-8.01* 10 ⁴ psi	0.775-1.9*10 ⁴ psi
UTS	28.3-100 ksi	7.01-10.5 ksi	2.9-4.35 ksi	5.5-7.5 ksi
Yield Strength (Elastic limit)	129-276 ksi	8.19-9.04 ksi	2.18-3.63 ksi	---
Multiaxial fatigue	---	2.8-4.2 ksi (at 10 ⁷ cycles)	0.834-1.02 ksi (at 10 ⁷ cycles)	---
Shear Modulus	4.35-4.69*10 ⁶ psi	0.144-0.216*10 ⁶ psi	0.02-.0276*10 ⁶ psi	---

After evaluating the possible biomaterials that were suitable for cardiovascular applications, the team decided to use polyurethane as the material for the cardiac scaffold. This decision was based on the material’s mechanical properties, biocompatibility, corrosion and wear resistance, cost, availability, and manufacturability to the team’s specifications.

Table 4: Qualitative Material Description

Material	Mechanical Properties	Bio/Hemo-compatibility	Corrosion & wear resistance	Availability	Ease of manufacturing
<u>Dacron</u>	may kink	Susceptible to fibrotic encapsulation and infection	Can degrade	✗	easy
<u>Nitinol</u>	Shape memory, strong	excellent	Oxide layer protects surface from corrosion and degradation	✓	fair
<u>ePTFE</u>	Change drastically over time	Can ward off infections	Can degrade	✓	fair
<u>Polyurethane</u>	Durable, resistant to fatigue, elastic and compliant to surrounding cardiac tissue	Not cytotoxic to cells, no thrombus formation observed, resistant to bacteria	Does not degrade over time (durable)	✓	easy

Table 5 shows the results stated above just as positive (+) and negative (-) signs to represent the material's performance under each category. The last column displays the total of positive signs for each material. The total numbers were used to evaluate the most appropriate material for the design of the scaffold. As seen in the chart results, polyurethane has the highest number of positive aspects; therefore, polyurethane is the best-suited material for the cardiac scaffold design.

Table 5: Material Summary

Material	Mechanical Properties	Bio/Hemo-compatibility	Corrosion & wear resistance	Availability	Ease of manufacturing	Total +
<u>Dacron</u>	-	-	-	-	+	1
<u>Nitinol</u>	+	+	+	+	-	4
<u>ePTFE</u>	-	+	-	+	-	2
<u>Polyurethane</u>	+	+	+	+	+	5

The polyurethane brand obtained for the purpose of our project was Chronoflex® C developed by AdvanSource Biomaterials. Chronoflex® C is an aromatic thermoplastic polyurethane especially designed for biodurability by preventing surface degradation caused by stresses from the surrounding environment (ChronoFlex, 2008). If needed, this material could be compounded for radiopacity (ChronoFlex, 2008), allowing the team to track the scaffold after implantation through imaging technologies. The implementation of Chronoflex® C in biomedical devices is not regulated under a specific FDA regulation (ChronoFlex, 2008) which would require a specific FDA approval for the team's application before human trials could commence. The full material analysis and AdvanSource's specification sheets on Chronoflex® C can be seen in Appendix C.

Material Processing

Once the Chronoflex® C polyurethane was acquired from AdvanSource Biomaterials, the group worked with Matt Phaneuf and Saif Pathan of Biosurfaces, Inc. (Ashland, MA). Matt and Saif were able to successfully electrospin the polyurethane pellets into thin microporous sheets. In order to provide the group with a sheet that was as close to the desired specifications as possible, there were several settings that had to be considered. One such setting was the distance from the needle to the collecting plate (a distance of 15cm was chosen for application). If this distance was increased, the result would have been thinner fibers and thinner pores. While electrospinning the material, a 10% weight to volume ratio of polyurethane was used. A 20kV voltage was applied to the polyurethane which was sprayed out at a rate of 3mL/hr. Polyurethane membranes were electrospun at three different time intervals: 30 minutes, 60 minutes, and 90 minutes (n=1 for each time). The average sheet thickness for a 60 minute electrospun sample was approximately 50µm.

Chapter 5: Design Verification

Culturing Mesenchymal Stem Cells

The following material is taken from the advice of Jacques Guyette, a PhD grad student in the Biomedical Engineering Department at Worcester Polytechnic Institute. Caring for the human mesenchymal stem cells requires diligent attention to detail. The first care item is preparation of media to sustain the cells. The media was prepared in the sterile hood and contains 500mL of DMEM as the base. To this 50mL of fetal bovine serum (FBS) and 5mL of PenStrep was added to create a 10% FBS and 1% PenStrep solution. The media, which needs to be replaced every 2-3 days, was placed in three 50mL conical tube aliquots and ten 15mL conical tube aliquots. The rest was left in the original DMEM container. The cells were grown in a T75 size flask which only required 8mL of media.

Human mesenchymal stem cells are attachment dependent. In order to remove them from their T75 flask and separate them into two flasks (or utilize for experiments) it was necessary to break down the extracellular matrix which holds the cells to the surface of the container. This was done by first removing the media in the flask and adding 7mL of trypsin to the cells; trypsin is a protease which breaks down protein (Guyette, 2008). After 10 minutes the flask was checked under the inverted microscope, and if, when agitated, cells were seen to shift and float, the solution was ready to be spun. It is important not to leave the trypsin activated with the cells for longer than 15 minutes. This is because the trypsin will begin to break down the cells themselves. The cells + trypsin were added to a 15mL conical tube with 4mL of fresh media. The fetal bovine serum in the media deactivates the trypsin. Putting this 11mL cell, deactivated trypsin, and media into a centrifuge with a counter weight, it was spun at a low velocity for 5 minutes. Upon taking the conical tube out of the centrifuge, the dilatant media is on top and the

cell pellet at the bottom. The dilutant was removed and 1mL of fresh media was added to the cell pellet. After the cells were re-suspended in the new media, the number of cells had to be counted. This was done by taking 10 μ L of the cell suspension and adding it to a small tube of 40 μ L trypan blue and 50 μ L of Phosphate-buffered saline (PBS). After mixing this mixture well, 10 μ L of the solution was carefully added to each side of a hemocytometer. The cells were counted in the hemocytometer using the inverted microscope.

Experimental Design

After the design criteria were identified and the materials had been selected, testing was necessary to ensure that the device would meet all requirements. The testing of medical devices must follow strict protocols established by the Food and Drug Administration (FDA), which classifies all medical devices into one of three classes. Class I devices are those that pose minimal harm, either to the patient or the user. Consequently, they require the least amount of regulatory control. Examples of Class I devices include bandages and latex gloves (Device Classes, 2002). Class II devices are those that pose potential harm, and thus require general and special controls. Special controls may indicate specific labeling requirements or specific performance criteria. Examples of Class II devices include powered wheel chairs and infusion pumps (Device Classes, 2002). Lastly, Class III devices are those that pose the most danger and thus require the strictest regulation. Premarket approval is required for most Class III devices before testing can commence. In order to gain premarket approval, an application must be filed and a review committee will then determine whether or not the device is safe and effective. Class III devices include any life-sustaining implant such as pacemakers and endosseus devices (Device Classes, 2002).

A cardiac scaffold implanted in the heart would be classified as a Class III medical device as it poses great potential harm. The implantation procedure itself is dangerous, and if the device malfunctions, the consequences of its failure could be fatal. Thus, in order to be approved by the FDA, the effectiveness of the device must be shown. Additionally, the device should be designed to be as safe as possible to diminish potential harm.

As with all Class III devices, the criteria the device must meet will be strict. Organizations such as the American Society for Testing Materials (ASTM) write standard tests that can be done to validate the properties of specific materials. The International Standards Institute (ISO) is another organization that writes standards that researchers, scientists, manufacturers and more must comply with in order to effectively bring a product to market (Ratner, 2004). This section identifies some of the tests and standards that a cardiac scaffold device must meet in order to obtain approval.

Preparing for Cell Assays

Prior to using the electrospun samples to carry out the Migration Assay, Cell Viability Assay, and the Connexin Assay, the group needed to sterilize the polyurethane sheets. This was done by first soaking them in 70% ethanol for approximately two hours. Afterwards, they were soaked in distilled water for two hours and allowed to dry in a sterile air hood overnight.

Furthermore, the group needed to have special wells manufactured in order to perform these assays. The group used a core design created by Professor George Pins (Worcester Polytechnic Institute, MA) where a sheet of material is clamped between two caps. The group altered the design slightly to increase the ease with which the wells could be manufactured, and then had Giacomo Ferraro (Worcester Polytechnic Institute, MA) machine the wells out of a

Lexan plastic. These wells, as seen in Figure 18 and termed “Gaudette-Pins wells”, are autoclavable and allowed for the group to carry out all the necessary assays.

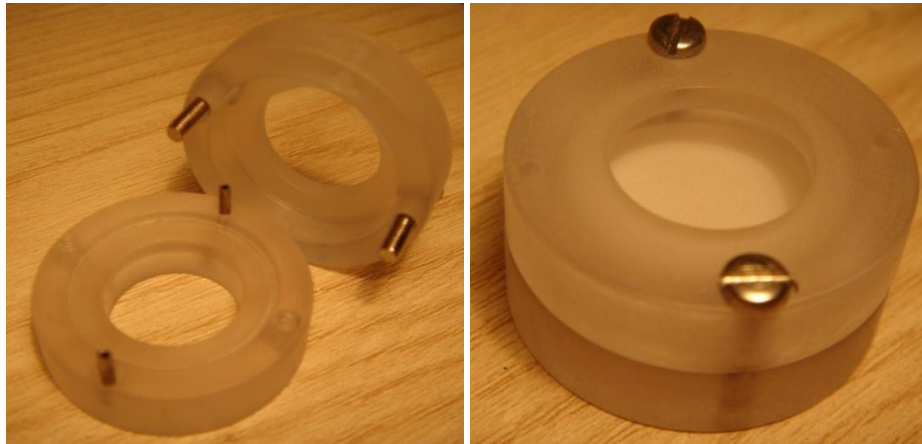


Figure 18: Custom built wells which house the polyurethane scaffold and allow for the seeding of cells on both the upper and lower side

Pore Size Migration Assay

Migration of non-terminally differentiated stem cells from target sites is a current concern around stem cell based therapies. In this context, the migration of modified hMSCs migrating away from the heart and differentiating could cause unpredictable effects on the body. A direct effect could be multiple concentrations of modified hMSCs settling at different sections of the heart. This could mean multiple action potentials initiating simultaneously at different locations of the heart resulting in fibrillation. For these reasons limiting and ideally preventing migration all together is a key function of the design.



Figure 19: Preliminary Design of Stem Cell Scaffold

To limit migration, the team proposed to create a porous mesh (See Figure 19). An integral aspect of this design is the pore size of the mesh. Ritter et. al, investigated the migratory

effects of Basic Fibroblast Growth Factor (FGF-2) on human mesenchymal stem cells (2008). In a Transwell migration assay (Boyden assay), they found hMSCs migrated through 8 μ m pores when FGF was used as a chemoattractant in excess of 20ng/mL. Although Ritter et. al, found that breast cancer derived FGF-2 and Vascular Endothelial Growth Factor (VEGF) both induced attractive migration of human mesenchymal stem cells, in vitro concentrations were similar and FGF-2 costs less to obtain (Invitrogen, Carlsbad, CA). In addition to 8 μ m pores, the team utilized 3 μ m and 0.4 μ m pore Transwells (NUNC, Rochester, NY) to determine the pore size at which hMSCs cannot migrate. See Figure 20 for test representation. A concentration of 30ng/mL placed in the lower compartment with 400 μ L of DMEM media simulated double the physiological concentration of FGF-2. 100,000 hMSCs were seeded on the upper part of the microporous membrane and incubated for 3 days at 37°C and 5% CO₂. Migration of cells was quantified using Hoechst and Phalloidin staining for cell nuclei and cytoplasm, respectively.

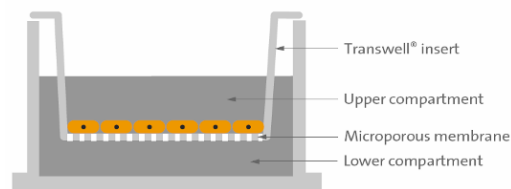


Figure 20: Pore Size Test (Corning Transwell® Permeable Supports)

Quantifying hMSC Migration

In order to quantify the results from the pore size migration assay, Hoechst and Phalloidin stains were used on both the wells and the well inserts to fluorescently label cells. The Hoechst stain was used to label the nucleus of the hMSC, while the Phalloidin stain identified the cellular cytoplasm. The following protocol was used to stain for stem cell migration:

1. Remove the well insert from the well and place into another sterile well. Rinse both in PBS solution for 5 minutes.

2. Remove the PBS solution and re-rinse both the well and the insert in PBS for another 5 minutes.
3. Remove the PBS solution. Place 4% paraformaldehyde at the bottom of the well and insert for a total of 10 minutes to fix the cells.
4. Remove the paraformaldehyde and rinse with PBS solution for 5 minutes.
5. Remove the PBS solution and re-rinse both the well and the insert in PBS for another 5 minutes.
6. Remove the PBS solution. Place .25% Triton-X (in PBS) onto the well and insert for a total of 10 minutes.
7. Remove the Triton-X and rinse with PBS solution for 5 minutes.
8. Remove the PBS solution and rinse with 1% Bovine Serum Albumin (BSA) in PBS for 10 minutes.
9. Remove the PBS/BSA and place Alexa Fluor 488 Phalloidin stain (5 μ L Phalloidin per 200 μ L PBS) on the samples for 30 minutes.
10. Remove the stain and rinse with PBS/BSA for 10 minutes.
11. Remove the PBS/BSA and re-rinse with more PBS/BSA for 10 minutes.
12. Remove the PBS/BSA and re-rinse with more PBS/BSA for another 10 minutes.
13. Remove the PBS/BSA and place Hoechst 3342 Trihydrochloride Trihydrate stain (10 μ L/1mL Distilled Water) on the samples for 5 minutes.
14. Remove the stain and rinse with PBS/BSA for 5 minutes.
15. Remove the PBS/BSA and place pure PBS onto the samples.
16. Examine the samples under a fluorescent microscope.

Scaffold Gap Junction Formation Assay

Another important aspect of the team's design is whether the hMSCs form gap junctions through the porous polyurethane. In order to test this, the team proposed to do another Transwell assay. The difference being that whereas the pore size was evaluated utilizing migration across industrial standard polycarbonate transwells, this assay looked at gap junction formation across a polyurethane microporous membrane. After the results of the pore size assay are complete, the team will know the range of pore sizes with which to construct the polyurethane scaffold. Instead of seeding a single cell layer on the upper portion of the porous membrane, it was necessary to have one layer of cells on each side of the microporous polyurethane membrane. See Figure 21 for assay representation. The cells needed to be geared towards gap junction formation. It would be ideal to place myocytes obtained from mice or dogs across from the hMSCs; however obtaining cardiac myocytes is difficult and maintaining in culture is also very challenging. Another option would be to obtain special connexin 43 expressing cells, but again these cells are delicate and expensive. The cost effective solution was to seed hMSCs on both layers. Using connexin 43 staining and confocal microscopy it was possible to determine gap junction formation across the pores. After seeding and the appropriate tracking (quantum dot) the system was incubated for 48 hours and stained for connexin 43. See Figure 21 for design specification of custom built dual well for gap junction assay.

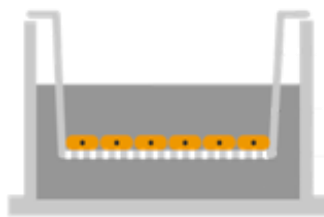


Figure 20: Two layers of hMSCs across a microporous polyurethane membrane

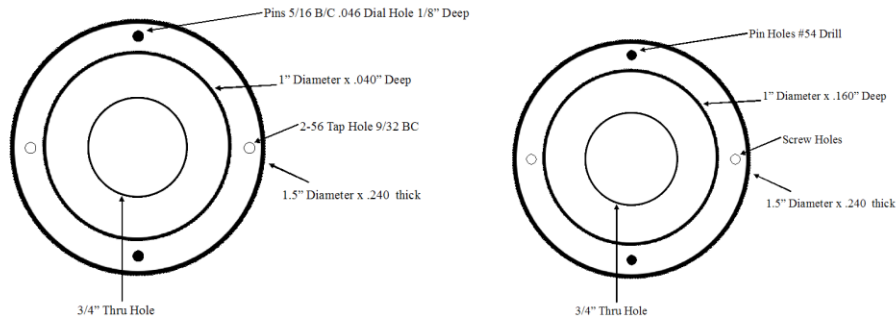


Figure 21: Gaudette-Pins Dual Transwell Design

Gap Junction and Live/Dead Immunohistochemistry

In order to determine whether gap junctions form between the polyurethane membrane, connexin 43 (the primary protein in gap junctions) staining was conducted. The following was the procedure for connexin 43 staining; Figures 22 and 23 are representative images of tissue controls and cell samples.

1. Fix cells in cold acetone for 10 minutes at -20°C
2. Rinse twice with PBS 5 minutes each wash
3. Rinse with Triton X for 10 minutes
4. Block with 1.5% Normal Rabbit Serum (NRS) at room temperature for 1 hour
5. Add primary anti-body (mouse anti-connexin) at 1:250 concentration in 1.5% NRS and incubate overnight at -20°C
6. Rinse 3 times with PBS for 5 minutes each
7. Add secondary anti-body (Alexa Flour 488 rabbit anti-mouse at 1:400 concentration in 1.5% NRS for one hour (Light Sensitive – Keep covered after this step)
8. Rinse with PBS 5 minutes
9. DAPI counterstain
10. Observe results

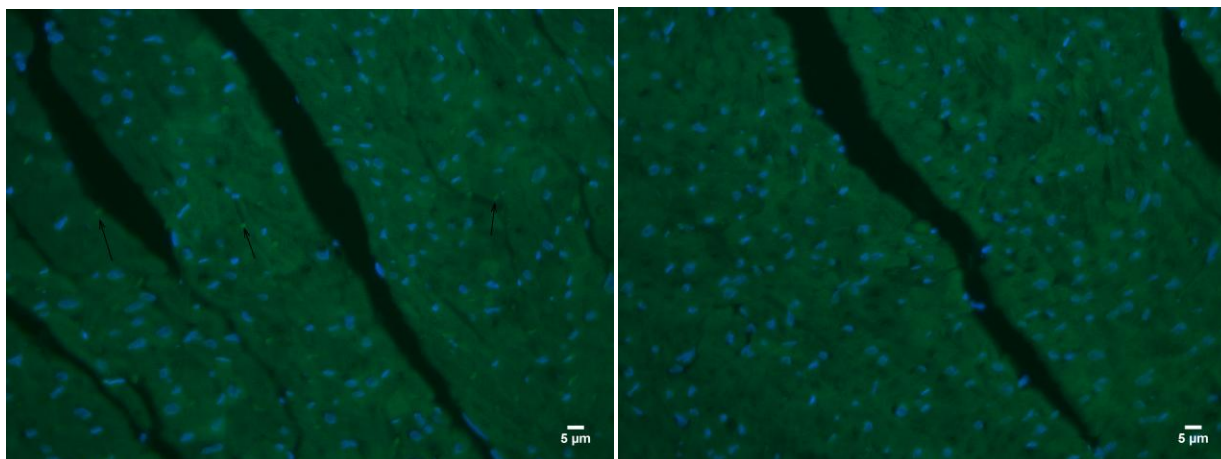


Figure 22: Positive (left) and Negative (right) Tissue Control Slides 40x

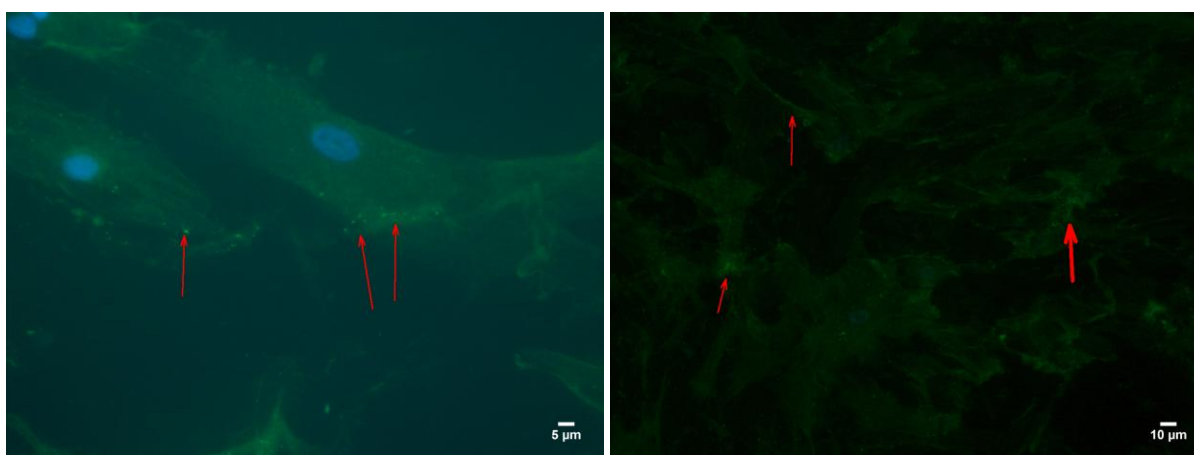


Figure 23: Positive Cell Samples at 40x (left) and 20x (right)

It was also necessary to determine cell viability on the polyurethane scaffold. To this end, the team performed Live/Dead staining. Proper concentrations for the solutions were previously determined by Jacques Guyette. For live hMSCs the fluorescent dye calcein was used at a concentration of 1µMolar. For dead hMSCs, Ethidium Bromide was used at a concentration of 8 µMolar. Figure 24 shows representative images of Live/Dead staining results. The following protocol for Live/Dead is very straightforward.

1. Create a combined solution of the two dyes in sterile PBS at the appropriate concentrations.
2. Add the solution to the cells

3. Cover
4. Incubate for 20 minutes at 37⁰C
5. Add fresh Live/Dead solution or PBS to wash cells.
6. Observe cells.

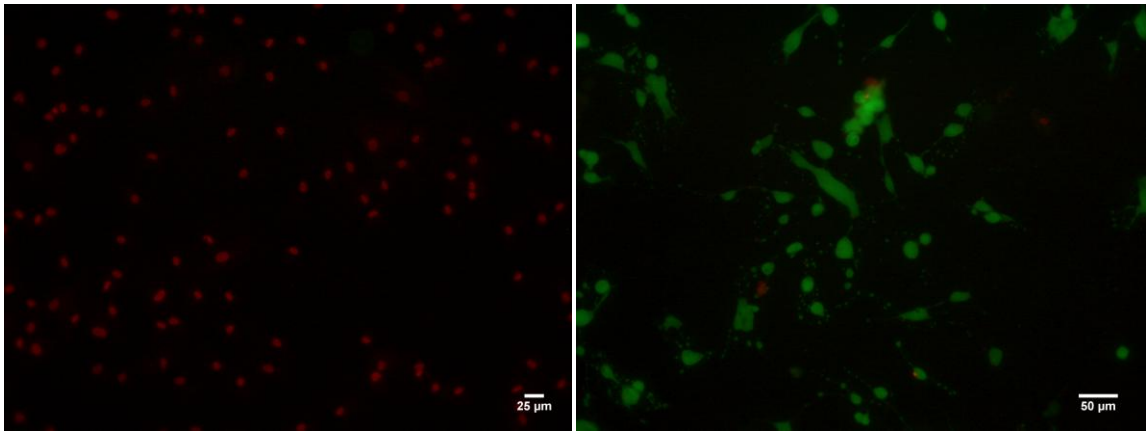


Figure 24: Sample Staining of Dead (left) and Live (right) cells

Chapter 6: Experimental Results and Discussion

Pore Size Migration Assay – Trial 1

For the first trial of the pore size migration assay, three separate items were stained: the bottom of the wells after 3 days of incubation, the bottom of the wells after 11 days of incubation, and the well inserts themselves after 11 days of incubation. Staining of the wells used for the 8 μ m pore inserts showed that only 3-4 hMSCs passed through after 3 days of incubation; however, after 11 days, a significantly larger amount of cells had passed through. In some of the wells, over 20 hMSCs had migrated through. With the 3 μ m inserts, only 1-2 cells were seen in the wells for both 3 and 11 days worth of incubation. Staining of the wells used in conjunction with the 0.4 μ m inserts showed no signs of cell migration. Figure 25 below shows some of the images that were obtained from the first trial.

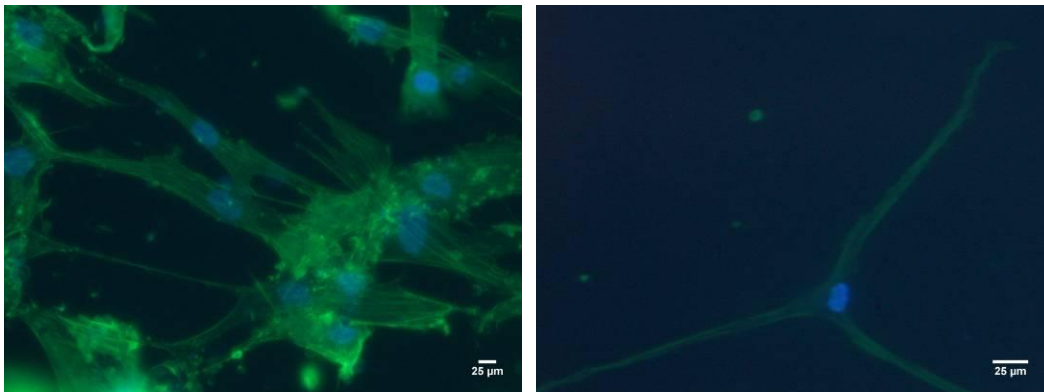


Figure 25: Bottom of 8 μ m insert (left) and bottom of well (right)

This trial helped to provide some supporting evidence as to the proper pore size for the scaffold. Based on the results, it appears that the proper pore size will be between 0.4 μ m and 3 μ m. While a minimal amount of cells passed through the 3 μ m pores, no cells seemed to pass through the 0.4 μ m pores, which suggests that the pore size will probably be around 1 μ m to 2 μ m.

While this data was informative, there were a couple of limitations with this trial. The first was that no controls were used. For the next trial, positive controls (wells with hMSCs seeded at the bottom) and negative controls (wells and inserts with just media) will be used so that the team can more subjectively determine cell migration.

Another limitation of this trial was that the bottom of the wells was used to quantify stem cell migration. Although this provided some information, hMSCs are attachment dependent; it is unlikely that a large amount of cells would detach and sink to the bottom of the well. The cells would be more likely to migrate through the pores to the other side of the well. Although these cells did not float away, they were still able to migrate through the pore size (meaning that a smaller sized pore would be needed for the scaffold).

In order to obtain more valid results, the second trial will also look at the bottom side of the well insert. The top part of the well insert will be scraped to remove any cells that did not migrate through, and then the remaining cells will be stained to identify migration. This methodology was effectively used by researchers who performed a similar transwell migration assay (Forte et al, 2006).

Once a proper pore size range has been confirmed, a similar assay will be conducted using a polyurethane scaffold instead of the polycarbonate well inserts. Scaffolds with various pore sizes will be used to ultimately determine what the necessary pore size must be.

Pore Size Migration Assay – Trial 2

The second trial of this assay had a similar setup to the previous run, but with only 0.4 micron and 3 micron porous wells. Again, a FGF based chemoattractant was used to help induce

migration of the hMSCs (approximately 55ng/mL) and roughly 50,000 cells were allowed to incubate within the wells for 3 days before the staining procedures were carried out.

The limitations associated with the initial trial of the Migration Assay were also addressed in this run. In order to have some experimental control, both a positive and negative control were used in order to more accurately identify the migration of a stem cell through a pore. For the positive control, hMSCs were seeded on the reverse side of the well; for the negative control, only media was put into the well.

The other major drawback with the initial trial was addressed in how the wells were analyzed. The initial run looked at cells which had completely passed through the well and seeded to the bottom of the plate. However, it is more likely for the stem cells to migrate from the upper side of the well to the lower portion through the porous membrane. In order to identify this style of migration, the wells were examined prior to and after scraping the upper portion of well membrane.

After completing the staining, the 0.4 micron wells were analyzed with an inverted fluorescent microscope. When examining the wells prior to scraping them, it was apparent that there were still cells on the membrane, either on the upper or lower surface. After scraping the upper surface with a q-tip, the wells were re-examined, which showed evidence of no cell migration to the opposite side of the well. Figure 26 contains representative images of the 0.4 micron wells, both before and after scraping.

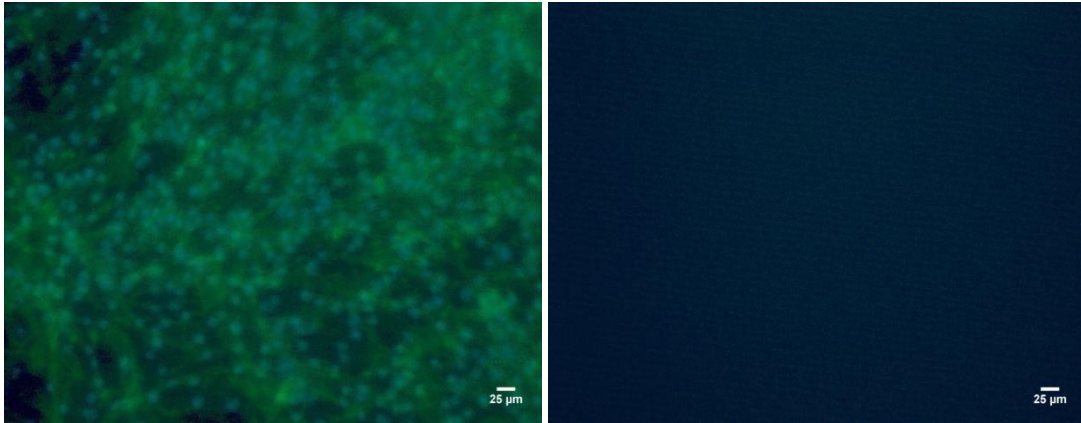


Figure 26: .4 micron wells prior to scraping (left) and post scraping (right)

Similar to the 0.4 micron wells, an initial look with the scope revealed a mass of cells on the 3 micron wells. However, after scraping the wells with a q-tip, there was still a significant amount of cells. This confirms the belief that the 3 micron pores are too large, which allow for the cells to migrate through to the other side. Figure 27 below shows the representative images.

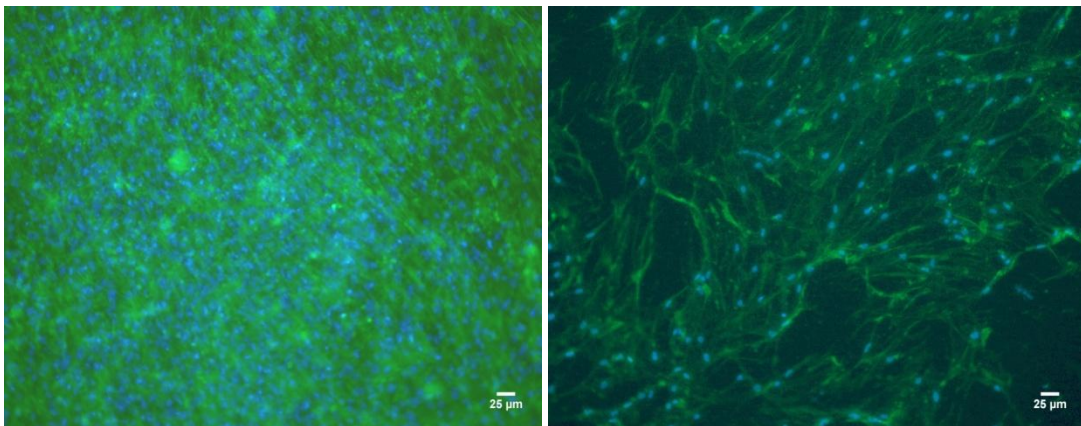


Figure 27: 3 micron wells prior to scraping (left) and post scraping (right)

Cell Viability Assay

The results from the cell viability assay showed a mixed bag of live and dead fluorescent signal. For the most part there was live signal as shown in Figure 28. The controls had a much brighter signal for both live and dead. Live signal is represented by green while dead cells show up as red. The polyurethane isn't completely transparent so it could have played a role in the reduced signal. In addition, the formation of gap junctions among the cells demonstrated cell viability on the polyurethane. The next section goes into detail about gap junction formation.

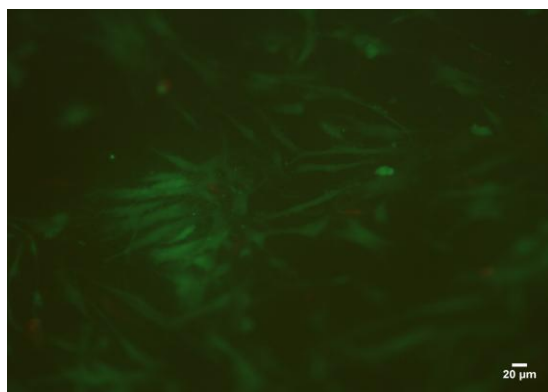


Figure 28: Live/Dead Results

Gap Junction Assay Results

Cells were seeded on both sides of the polyurethane scaffold suspended in the Gaudette-Pins dual well and allowed to incubate for 48 hours. Staining with controls was conducted as outlined in the methodology. Confocal microscopy was used to determine gap junction formation through the polyurethane. Confocal microscopes allowed for visualization in the x-, y-, and z-planes, Figure 30 shows a 3-D projection of the cell seeded polyurethane. The nuclei (blue circles) on the far sides represent cells on opposite sides of the polyurethane. As seen in Figure 29 there is nuclei signal and gap junction (green) signal *between* the polyurethane scaffolds. The results demonstrate that formation of gap junctions through the scaffold is possible.

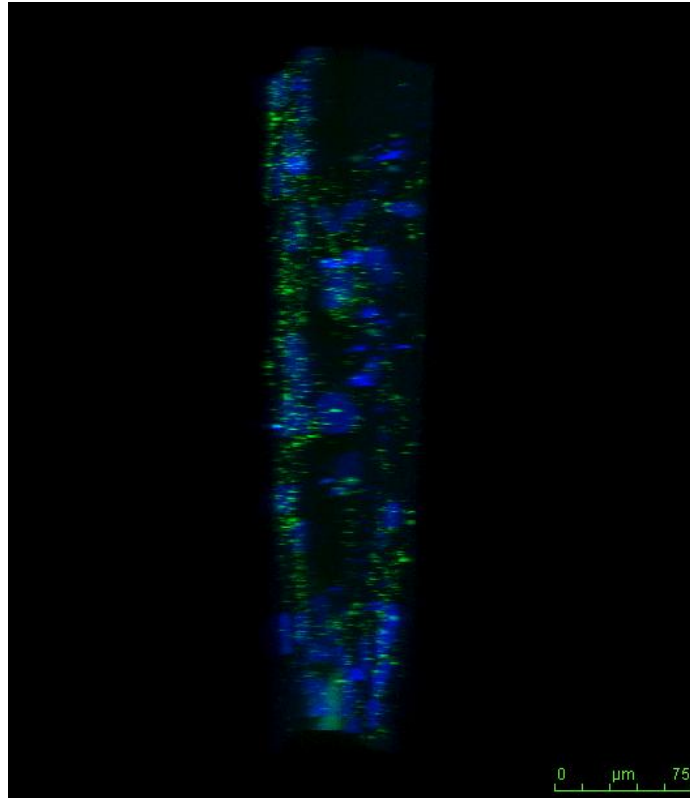


Figure 29: 3D Gap Junction Formation through Polyurethane

Migration through Polyurethane

As stated, one of the potential limitations with the electrospun polyurethane is the lack of a precisely controlled pore size. In order to ensure that the gap junctions seen in the previous assay were formed through a barrier that limited migration, another migration assay was conducted. All test parameters remained the same, except this time the specially manufactured wells were used. Quantifying migration for this round of experiments was less complicated because the polyurethane sheets were not transparent. Therefore, no scraping was necessary; when being examined with the fluorescent scope, the group could just flip over the custom made well to examine the other side.

Overall, results from the test showed that no cells were able to pass through the 30, 60, or 90 minute electrospun microporous sheets. This means that the settings with which Biosurfaces, Inc. electrospun the polyurethane would prevent migration of the cells and allow for the formation of gap junctions. Figure 30 shows the difference between the side of 60 minute sheet on which cells were seeded, and the opposite side (where the hMSCs could not migrate to).

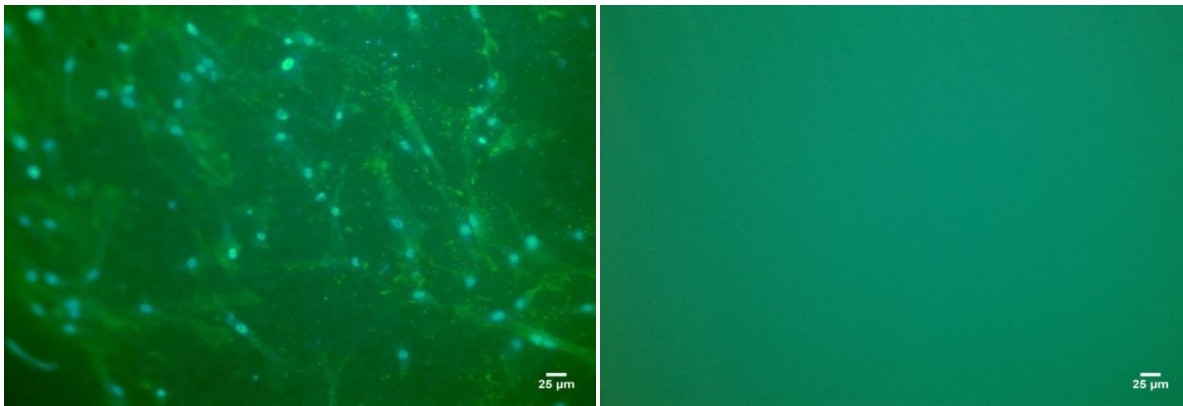


Figure 30: Human Mesenchymal Stem Cells on one side of the polyurethane sheet after 3 days of incubation (left); Reverse side of the same polyurethane sheet, where no cells were able to migrate to (right)

Mechanical Calculations

Deflection of a hMSC

Based on the pore-size testing results, the pore size of the electrospun polyurethane should be between $0.4\text{-}3.0\mu\text{m}$. However, this is a wide range and doesn't provide a specific enough result; therefore, to obtain a better pore-size approximation, the deflection of an hMSC was calculated mathematically at different pore-sizes.

The main importance of these calculations was that it allowed the design team to determine what the fiber diameter should be of the electrospun polyurethane. In order for gap junctions to occur, both the pore size and fiber diameter had to be balanced so that cells on opposite ends of the fiber deflect and touch each other. If these two parameters are not appropriately balanced, either the cells will not come into contact with each other or the cells will migrate through to the opposing end of the fiber.

To begin the calculations, it was assumed that the cell was in the shape of a beam. From literature, it was determined that a cell has a length of $10.0\mu\text{m}$ and a thickness of $2.0\mu\text{m}$ (Tastan, et. al., 2009). It was also assumed that there was a uniform load distribution on the cell caused by the beating heart (see Figure 31).

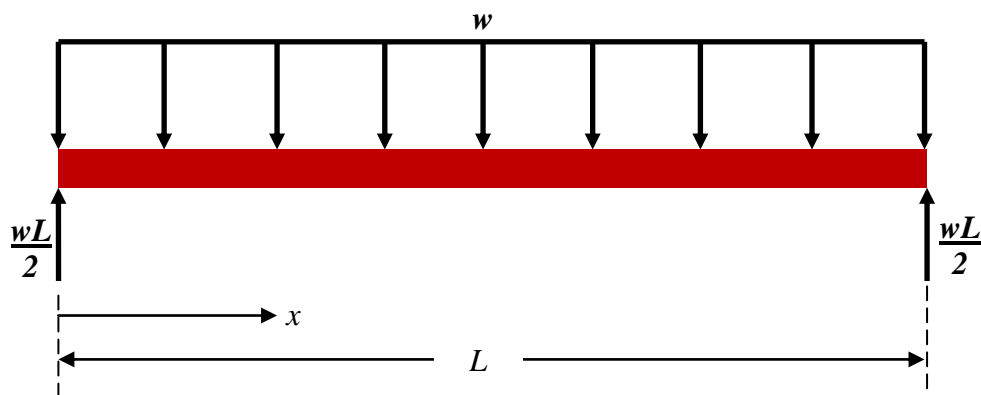


Figure 31: Free Body Diagram of a hMSC

As part of the derivation for deflection, the maximum deflection would occur at $x = \frac{L}{2}$;

based on this, the maximum deflection equation is:

$$Eq. 1 \quad \Delta_{max} = \frac{5wL^4}{384EI},$$

where E is the Young's Modulus of a hMSC, I is the moment of inertia of the hMSC, L is the length between fibers (the pore-size), and w is the force per unit length (see Appendix D for full derivation). The constants obtained from literature were Young's Modulus and the pressure exerted by the intramyocardial wall. In a study conducted by Tan, et. al. (2008), it was determined that at human body temperature (37°C), the Young's Modulus of an hMSC is 126±81Pa. For the intramyocardial pressure constant, Heineman et. al. (1985) determined that there was a range of 5±2mmHg. The mean value (5mmHg) was then used to determine the force per unit length exerted onto the cell at various pore sizes.

To calculate the moment of inertia, it was assumed that the shape of the cell was elliptical. For a quarter of an ellipse, the moment of inertia equation is:

$$Eq. 2 \quad I = \frac{\pi ab^3}{16},$$

where a and b are defined in Figure 32.

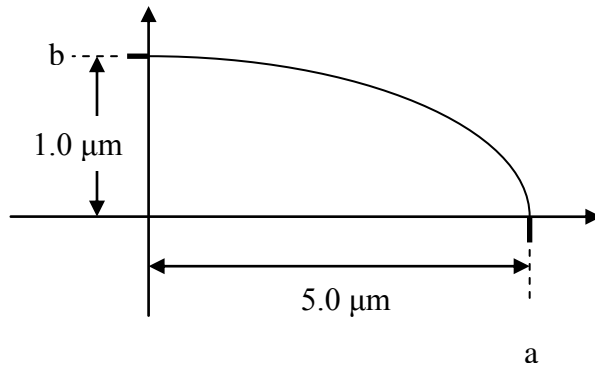


Figure 32: Moment of Inertia of a hMSC

This equation was modified in order to calculate the moment of inertia of a full ellipse. To do this, the quarter ellipse equation was multiplied by four, which resulted in the following equation:

$$Eq. 3 \quad I = \frac{\pi a b^3}{4} .$$

After the variables a and b were plugged into the former equation, the resulting moment of inertia of a hMSC is $3.93\mu\text{m}^4$.

The last variable included in the maximum deflection equation, L, varied from 0.4 to $3.0\mu\text{m}$. For the calculation, increments of 0.5 were used from 1.0 to $3.0\mu\text{m}$; no increments were used between 0.4 and $1.0\mu\text{m}$.

The calculations for the maximum deflection were completed using MatLab. An example of the syntax used in MatLab is shown in Figure 33. For all MatLab coding, see Appendix E.

```

For L=3.0 micrometers
%E=45Pa
E=45*(1/((1*10^6)^2)); %N/micrometer^2
L=3; %micrometer
a=5; %micrometer
b=1; %micrometer
w=(266.6*(1/((1*10^6)^2))*25*pi)/3; %N/micrometer
I=(pi*a*(b^3))/4
    %I=3.927 micrometers^4
d=(5/384)*((w*(L^4))/(E*I))
    %d = 41.6563 micrometers

```

Figure 33: MatLab Syntax

Upon completing all the calculations, the team decided the most desirable pore-size would be between 2.0 and $2.5\mu\text{m}$ (see Table 6; for all results, see Appendix F) because it would result in a more manageable fiber thickness. The average deflection length between 2.0 and $2.5\mu\text{m}$ is $15\text{-}30\mu\text{m}$. Therefore, the fiber diameter would need to be double the deflection length in order to account for cells deflecting on opposite sides of the fiber and forming gap junctions. As a result, the fiber diameter should be approximately $30\text{-}60\mu\text{m}$.

Table 6: Calculation Results

Length between Fibers = 2.0 μm			Length between Fibers = 2.5 μm		
Pressure (Pa)	E (Pa)	d (μm)	Pressure (Pa)	E (Pa)	d (μm)
133.3	45	6.16	133.3	45	12.03
	126	2.2		126	4.3
	207	1.34		207	2.61
266.6	45	12.34	266.6	45	24.11
	126	4.41		126	8.61
	207	2.68		207	5.24
666.6	45	30.86	666.6	45	60.28
	126	11.02		126	21.53
	207	6.71		207	13.1
799.9	45	37.03	799.9	45	72.33
	126	13.23		126	25.83
	207	8.05		207	15.72

a) Calculation results for L=2.0 μm

b) Calculation results for L=2.5 μm

Figure 34 represents the correlation between the length between fibers and the Young's Modulus. As the pore size increases, the deflection also increases; as Young's Modulus increases, the deflection decreases.

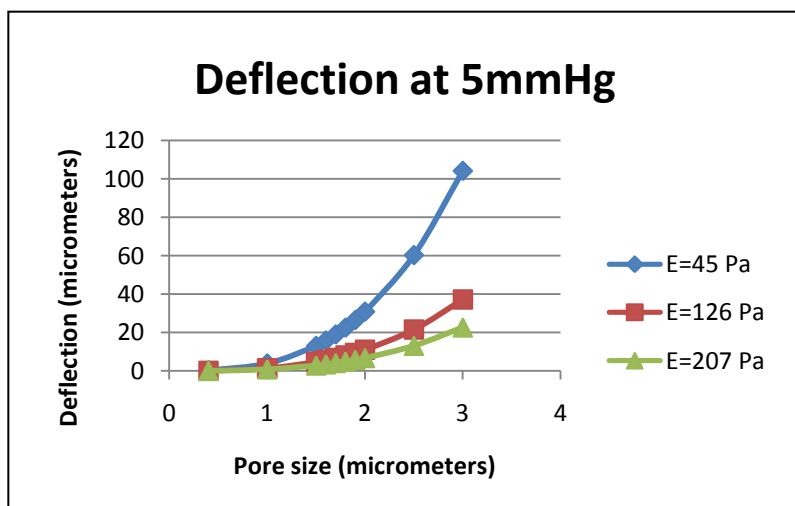


Figure 34: Deflection vs. Pore Size and Young's Modulus

Cell Quantity Threshold

The design team contacted Dr. Ira Cohen of SUNY Stony Brook University via e-mail to inquire about the number of modified hMSCs required to replace the function of the sinoatrial node. He responded that his team estimates 350,000 cells fully restore function, but with only 50% transfection efficiency they inject 700,000. In order to have a safety factor of two, the team decided to seed 700,000 onto the scaffold. Therefore, the area of the collected cells and the surface area of the scaffold both needed to be calculated to determine appropriate dimensions for the scaffold.

To calculate the area of a cell, the diameter of a cell used was 10 μ m, as used in the deflection calculations. The following formula was used to determine the surface area needed for 700,000 cells:

$$Eq. 4 \quad A_{cell} = \pi r^2 * 700,000 .$$

The calculated surface area was 55.0 mm² for 700,000 cells.

Economic, Environmental, and Ethical Impacts

While this project solely focused on the concept of limiting migration of stem cells, if the overall technology and research of a biological pacemaker reaches the point where it can be used effectively to pace the heart, it would allow for patients to undergo one surgery to fix any arrhythmia problems. This reduces the overall impact on the health care and economic system, since the cost of repeated surgeries to replace pacemakers would be decreased.

Overall, the cost of producing a biological pacemaker is less than that of the artificial pacemaker; therefore, the benefits of this product can reach people who may not normally have

been able to afford it. This would positively impact people not only in this country, but around the world as well.

As for environmental concerns, there are no major environmental impacts that result from this product. The overall cost of production and the cost of material is minimal when producing this product. Also, the biological pacemaker works with the body, so once the scaffold is produced and implanted; it does not need to be replaced. That way, there are no pacemakers or batteries to discard.

Lastly, the ethical considerations revolving around human mesenchymal stem cells are minimal since they are taken from each individual pacemaker. If the system revolved around embryonic stem cells, the ethical debates would be more significant.

Chapter 7: Final Design

Based on initial migration assays, the mechanical calculations, considerations for minimally invasive delivery through a catheter, and development of the team's preliminary designs; the team proposes the final design seen in Figure 35. The design consists of a two part cylindrical scaffold. The cylindrical shape was chosen because it resembled the shape of stents, which are widely used in the cardiac industry. The blue section is a solid cylinder composed of ChronoFlex® C. The purpose of this solid cylinder is to provide mechanical support to the scaffold. The red section represents a porous electrospun ChronoFlex® C film on which the modified hMSCs are seeded. This membrane is thin enough to allow for cellular communication across the scaffold and the pores are sized to prevent cells from migrating through to the other side. The team worked with Biosurfaces, Inc., who made the electrospun ChronoFlex® C membrane for this project. After cellular adhesion, the porous film is wrapped around the solid polyurethane cylinder. To finalize the scaffold, sealing bands and caps in conjunction with BioGlue® are added to prevent hMSC migration out of the scaffold from the sides of the cylinder. Another function of the sealing bands and caps is to protect the porous membrane from the shear stresses the scaffold might experience during delivery.

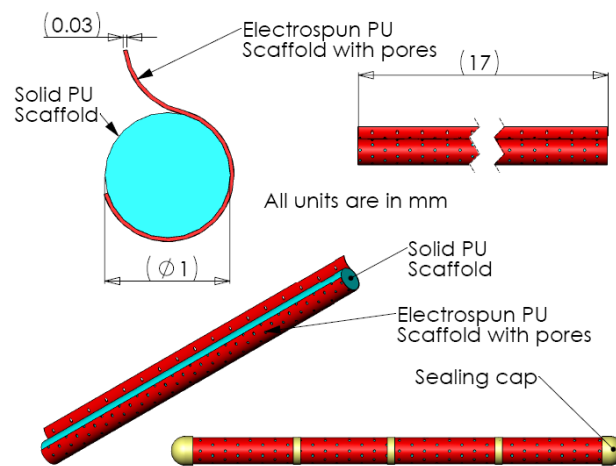


Figure 35: Final Design Representation

Following the recommendation of Professor Glenn Gaudette and using current cardiac catheter sizes as a guide to develop the scaffold, the team chose an outer diameter of 1.0mm for the solid polyurethane component of the design. The minimum length of the scaffold was then calculated taking into consideration the amount of surface area needed to seed 700, 000 cells (amount of cells seeded to induce pacemaker function in the heart) onto the surface of the porous membrane. Because the electrospun polyurethane is in the shape of a cylinder; the following surface area equation was used:

$$Eq. 5 \quad SA_{cylinder} = 2\pi r^2 + 2\pi r l ,$$

where r is the radius of the solid polyurethane scaffold, SA is the surface area of the 700,000 cells and l is the minimum length of polyurethane needed. After the variables were plugged into this equation, it was determined that the length needed was 17.0 mm.

The deflection calculations determined that the desired electrospun membrane thickness was between 30 and 60 μ m, and from both the deflection calculations and the pore size migration assay it was determined that the appropriate pore size was between 2.0 and 2.5 μ m.

Fibrin Glue

In order to seal the scaffold, the team plans to use sealing bands and caps in conjunction with BioGlue®. BioGlue is a surgical adhesive developed by CryoLife that has been specially designed for the use in cardiovascular surgery. It is composed of purified bovine serum albumin (BSA) and gluteraldehyde that are packaged in two separate chambers of a syringe as shown in Figure 36 (CryoLife, 2008).



Figure 36: BioGlue® syringe (CryoLife, 2008)

When the BioGlue is delivered, the two components mix and create a chemical reaction that causes the two materials to cross-link. The molecules of glutaraldehyde bond with the BSA molecules and when the mix becomes in contact with the proteins at the repair site, it creates a flexible mechanical seal that does not depend on the body's clotting mechanism (CryoLife, 2008).

The advantage of using this adhesive is that it starts to polymerize within 20 to 30 seconds after mixing, and at two minutes, it is strong enough to bond things together. This adhesive is useful for bonding biological tissue as well as synthetic grafts because it bonds within the interstices of the graft matrix (CryoLife, 2008).

Chapter 8: Conclusions & Future Recommendations

The results of this study showed that the electrospun polyurethane can serve as an effective scaffold to keep the hMSCs of a biological pacemaker in one centralized location. Not only did the polyurethane scaffold successfully inhibit stem cell migration, it proved to be an adequate environment for cell viability and gap junction formation.

For future work, the team recommends further research regarding the sealing of the scaffold around the solid cylinder. Once this problem has been addressed, the team believes that the scaffolds can be assembled and used in *in vivo* studies. Another area of future work also includes development of a catheter delivery system.

Another potential area of research could be regarding casting of polyurethane with micro-particles in order to create a controlled pore size. Although the electrospun scaffold was successful in preventing migration of the stem cells, there is a lack of a definitive pore size.

Mechanical testing regarding the strength of the scaffold needs to be performed in order to ensure it can withstand the contractile forces within the heart. Also, in terms of catheter implantation, it is necessary to determine if the scaffold can withstand the shear stresses it will be subjected to.

Appendix

Appendix A: Completed Pairwise Chart

The two pairwise comparison charts were sent to and filled out by Professor Glenn Gaudette, Jacques Guyette, Joseph Dell'Orfano, MD, and Ira S. Cohen M.D., Ph.D. Once returned, the design team filled in the corresponding gray boxes; if a white box (located horizontally) had a “0”, then the corresponding gray box (located vertically) would receive a “1”. The totals were then calculated for each row (see Table 2 for example).

Completed Pair wise Comparison Chart

PWCC 1st degree functions	Degradability	Biocompatibility	Immobilization	Allow Gap Junction formation	Myocardium attachment	Mechanically stable	Total
Degradability	0	0	0	0	0	0	0
Biocompatibility	1	0	1	1	1	1	5
Immobilization	1	0	0	0	0	0	1
Allow gap junction formation	1	0	1	0	1	1	4
Myocardium attachment	1	0	1	0	0	1	3
Mechanically stable	1	0	1	0	0	0	2
Total							15

To calculate the percentage of importance for each function, the averages were first taken for each row from each respondent. For example, if the four totals for degradability were 2, 3, 2, and 0, the average would be:

$$\frac{2 + 3 + 2 + 0}{4} = 1.75$$

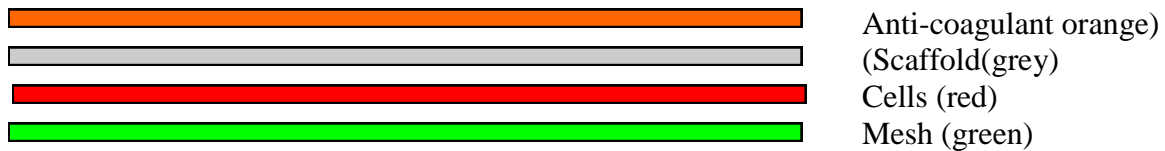
Appendix B: Conceptual Designs

Bag – There is a material (mesh, porous polymer, porous metal, porous ceramic) that contains the hMSCs in a spherical shape

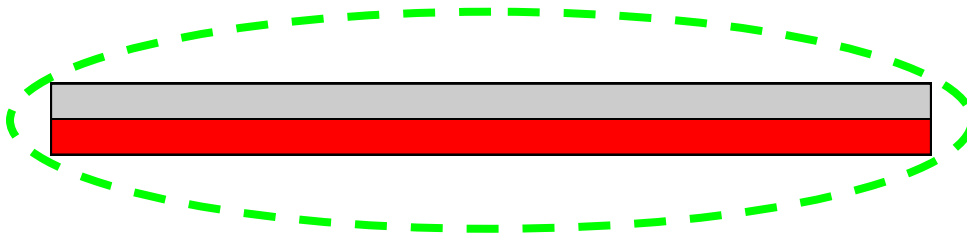


Pancake Discs

Four layers of disc attached to the ventricular wall. (Anticoagulant Coating facing ventricle, scaffold, cell layer, mesh inhibiting cell migration)



Three-Layered mesh bag attached to the ventricular wall (blood compatible mesh encompasses both cells and attachment scaffold)



Bi-Layer Pancake Cap



Flat Mesh Container



Open sided patch – attachment dependent hMSCs stay on scaffold, free side to interact with myocytes



Appendix C: Candidate Material Analysis

Nitinol

The first material that is being considered is nitinol. Nitinol was originally developed by the space program Nickel Titanium Naval Ordnance Laboratories (Whittaker et al, 2006). Nitinol is a passive shape memory alloy made from 55% Nickel and 45% Titanium (Trepanier et al, 2000) that is commonly used in the Biomedical Engineering industry. Some of the most frequent applications of nitinol involve vascular stents, orthopedic and orthodontic applications (Trepanier et al, 2000) such as arch wires and osteosynthesis plates (Pelton et al, 2000), and it is also used devices used in minimally invasive surgery like tissue ablation devices, vena cava filters and retrieval baskets (Pelton et al, 2000).

Nitinol can withstand a maximum strain of up to 8% without permanent deformation (Pelton et al, 2000); this attribute is usually referred to as super-elasticity. The material's super-elasticity and shape memory properties allow engineers to easily anneal the alloy to a certain shape that is then retained. The material can easily be cooled down and deformed in order to comply with the engineers' needs and when later reheated or simply brought back to room temperature, the alloy goes back to its annealed shape. This can be very useful when designing for implantation or for tool versatility.

A great attribute exhibited by nitinol that makes it appropriate for blood contacting devices, more specifically vascular applications, is the material's anti-thrombogenic properties and corrosion resistance. Extensive research done on the material has demonstrated its biocompatibility and leading to its approval by the FDA. The corrosion resistance of nitinol is attributed to a stable surface oxide layer that protects the material from its surrounding environment and increases biocompatibility. This is achieved by changing nitinol's chemical pathway of oxidation (Trepanier et al, 2000). As part of the design, scratching of the oxide layer must be kept at a minimum; especially when considering delivery of the device possibly through a catheter. If the oxide layer is disrupted this can affect nitinol's corrosion resistance properties. (Trepanier et al, 2000)

When testing for biocompatibility, the experiments were designed under the ISO 10993 standards. The properties of the material that are usually evaluated to assess biocompatibility include foreign body reaction, inflammatory response, thrombosis, carcinogenesis, sterilization and infection, (InspiredMD Corporation, 2005) as well as mechanical properties like fatigue testing. One risk of using biomaterials that contain nickel is the possibility of nickel ions being released into the body. It is known that nickel is a potent inflammatory agent in biological tissue (Whittaker et al, 2006), and excess release of nickel from the implant can cause harmful allergenic, toxic and carcinogenic reactions (Trepanier et al, 2000). Recent studies show that the maximum concentration of Ni released by nitinol is 4.1 ppb; and this takes place within the first 24 hours after implantation. For Ni to reach cytotoxic levels in the human body, it needs to reach a concentration of 30ppm (Jia et al, 1999).

Other experiments have been conducted to further evaluate the biocompatibility of nitinol. One concern for our project is fibrotic encapsulation of the biomaterial. If fibrotic encapsulation of our scaffold were to occur, then the cells seeded inside of the scaffold will not be able to form gap junctions with the cardiomyocytes located at the other side of the membrane. A study performed to understand the tissue reactions when nitinol is implanted subcutaneously showed that the inflammatory response of the body to the nitinol started 3 days after implantation and was minimal. The healing process, which consisted of fibrous encapsulation of

the biomaterial, started 1-2 weeks after implantation. (Trepanier et al, 2000) During the initial stages of wound healing, the fibrotic encapsulation thickness of nitinol is higher than stainless steel. As time goes on, the fibrotic encapsulation thickness of stainless steel increases and nitinol's remains the same. This results in both materials having the same fibrotic encapsulation thickness which makes nitinol biocompatible (Ryhanen et al, 1998). Although nitinol is considered a biocompatible material and very suitable for biomedical applications there is concern of how the fibrotic encapsulation of the material during the healing process will affect the outcome of the project. The group needs a material that will limit or completely resist fibrotic encapsulation in order to allow gap junction formation between the mesenchymal stem cells and the cardiomyocytes. Nitinol has great potential due to its mechanical properties, corrosion resistance and biocompatibility. Another great characteristic of nitinol is that it is radio opaque. This brings the opportunity of tracking the device due to its imaging possibilities (Whittaker et al, 2006).

Due to the material's hardness and the abrasive nature of its surface, machining parts out of nitinol causes a great amount of tool wear. This in turn makes processing nitinol more expensive and more time consuming than other materials. A disadvantage of nitinol is that its mechanical properties are decreased when welded onto itself or another metal. More detail on specific mechanical properties of nitinol can be found on the table at the end of this section.

Dacron

The second material that is being evaluated is Dacron, also known as Polyethylene terephthalate (PET). Dacron is tough, strong and is fairly easy to shape. It is also easy to join and sterilize. This material is composed of tiny woven or knitted fibers that have very high tensile strength (Sarkar et al, 2006) and is mainly used in the Biomedical Engineering industry as vascular grafts.

Dacron is usually manufactured into a woven corrugated graft, this is needed in order to prevent the material from kinking (Sarkar et al, 2006). This material design allows it to withstand the pressures exhibited by high flow blood vessels like the aorta (Sarkar et al, 2006). Since this material is used as a vascular graft it means that it is both biocompatible and hemocompatible. Dacron is chemically stable and resistant degradation and to toxic or even inflammatory byproducts that it might encounter in the blood. The individual fibers are susceptible to slow hydrolytic degradation, but the structures that are formed when the fibers are bundled prevent this process (Sarkar et al, 2006). Studies suggest that one disadvantage of Dacron is that it is prone to infection (Kajiwara et al, 2004). It can be woven or knitted to produce a porous fabric (InspiredMD Corporation, 2005), which might be advantageous for the team. Dacron, if manufactured with velour construction is believed to facilitate tissue incorporation which may work for the team's advantage when designing for gap junction formations. More detail on the material's mechanical properties can be found on the table below.

EPTFE

The next material studied is ePTFE or expanded PTFE. Expanded PTFE was developed in 1972. Preferred over Dacron for vascular applications (InspiredMD Corporation, 2005), EPTFE is considered the most reliable synthetic material available for vascular grafts (Doble et al, 2008). EPTFE was first introduced in the market as a vascular graft in 1975, early studies done on the material led to the addition of reinforcing fibers for stability of the graft (Isaka et al,

2006). ePTFE grafts currently available in the market are resistant to compression and kinking (InspiredMD Corporation, 2005).

A study that followed young patients (7-8 years old) showed that the mechanical properties of the ePTFE grafts changed between 10 and 52 weeks after implantation. The study revealed that the strength of the material was decreased by 50%, the material elongation changed by 61% and its crystallinity changed by 3% (Doble et al, 2008). The ultimate tensile strength of normal a normal ePTFE vascular graft was 14.57 MPa, after being implanted into the body for a few years the ultimate tensile strength of the material decreased to 7.25 MPa (Doble et al, 2008). The loss of mechanical strength of ePTFE was also demonstrated by Vanmaele et al., in this experiment the results showed to be as drastic as the loss of mechanical strength a week after implantation (Isaka et al, 2006). Some researchers attribute the loss of mechanical properties to the deposition of lipids and proteins on the graft wall (Doble et al, 2008). In an experiment carried out by Geiger, the structure of the ePTFE graft appeared to be inhomogeneous with micropores, and compressed and ruptured fibrils. (Geiger,1991)

So far there are no reported failures due to degradation of the material (Giudiceandrea et al, 1998), but this drastic change of ePTFE's mechanical properties could lead to further complications especially if implemented for long term implants.

One of the chemical characteristics of this graft is that it is hydrophobic. This quality of the material protects the ePTFE graft against bacterial adhesion, resulting in the ability to ward off more infections than other synthetic grafts like Dacron (Kajiwara et al,2004). Studies show that as blood proteins accumulate in the wall of the graft, this hydrophobicity fades away (Doble et al, 2008), and with this, the material's ability to fight infections. This makes the ePTFE grafts more susceptible to infections (Kajiwara et al, 2004). Other problems identified with these types of grafts are serum leakage, thrombosis, inflammation mineralization and changes in the physiochemical characteristics of the material (Doble et al, 2008).

The manufacturing process of ePTFE grafts can be used to control the physical dimensions of the material (Isaka et al, 2006). When the graft is not woven or knitted, it can be produced into sheets by an extrusion process. This extrusion process results in a porous membrane in which the pores can be controlled and produced to a desired size (InspiredMD Corporation, 2005) (Isaka et al, 2006). Expanded PTFE membranes have been previously manufactured with pores as small as .05 microns (Sarkar et al, 2006). This material is advantageous to the team because the pore sizes we are investigating range from 3 -.4 microns. It might be possible to produce an ePTFE membrane with the required pore size for our design, although the material's decrease of mechanical strength and biocompatibility after implantation are a concern.

Polyurethane

The last material investigated was Polyurethane. From the biomaterials that are available in the market today, polyurethane is considered the most biocompatible and hemocompatible materials. (Zdrahala et al, 1999). The most common brands available in the market for medical purposes are Pellethane™, Estane™, Vialon™, Tecoflex™, Corethane™, Bionate™, Biospan™ and Chronoflex™. (Zdrahala et al, 1999) These materials dominate the field of cardiovascular devices (Zdrahala et al, 1999)and are generally used in the biomedical engineering industry to make catheters, general purpose tubing, blood bags, heart valves, pacemaker lead wire insulation, wound dressings, total artificial hearts and small caliber vascular grafts. (Zdrahala et al, 1999)(Boretos et al, 1967) (Alliance for the Polyurethanes Industry, 2001)

Polyurethane's popularity comes from its great mechanical properties. By modifying polyurethane, scientists were able to obtain a material that is durable, resistant to fatigue in tensile, compression and shear stresses; a material that is elastic, compliant to surrounding tissue and due to attachment of certain proteins even able to encourage healing. (Zdrahala et al, 1999) Unlike ePTFE, tests performed on polyurethane's tensile properties after implantation showed that there was no significant reduction of the material's ultimate tensile stress (Boretos et al, 1967). The table below shows more detail on the material's mechanical properties.

When evaluating polyurethane's biocompatibility, tests showed that the material is not cytotoxic to cells. (Vinoy et al, 2008). This is very important for the purpose of our project because our intension is develop a scaffold in which we can seed cells. Observations made on polyurethane vascular grafts after 1 week implantation time showed no thrombus or emboli formation. (Boretos et al, 1967) this makes the material appropriate for blood contacting applications. MacKay et al showed in 1996 that how modifying polyurethane can give it excellent blood compatibility. By adding proteins on the surface of the biomaterial, it is possible to give it anticoagulant, infection controlling and tissue suppressant characteristics. Some of these modifications also gave polyurethane enhanced wound healing characteristics. (Zdrahala et al, 1999). A study conducted by Martinez-Martinez, demonstrated that polyurethane had the lowest adhesion and colonization of bacteria when compared to Teflon and silicone latex. (Zdrahala et al, 1999)

There are many processes that can be used to fabricate medical devices from polyurethanes. Among those processes we can find extrusion, molding, casting electrostatic and wet spinning of monofilaments, dip coatings and spraying of mandrels. The advantages of these manufacturing processes are that they can fabricate membranes with micropores that feel and behave like natural tissue. (Zdrahala et al, 1999)

ChronoFlex Technical Data Sheet

Properties	ASTM Procedure	Typical Values		
		80A	55D	75D
Hardness (Shore Durometer)	ASTM D-2240	80A	55D	75D
Appearance	Visual	Clear to slightly cloudy	Clear to slightly cloudy	Clear to slightly cloudy
Ultimate Tensile Strength (psi)	ASTM D-638*	5500-6500	6000-7500	7000-8000
Ultimate Tensile Strain (%)	ASTM D-638*	400-490	365-440	255-320
100% Secant Modulus (psi)	ASTM D-638*	770-1250	1850-2200	5300-5700
300% Secant Modulus (psi)	ASTM D-638*	700-1400	1700-2000	2700-3200
Flexural Strength (psi)	ASTM D-790	350	550	10,000
Flexural Modulus (psi)	ASTM D-790	5500	9300	300,000
Melt Index (g/10 min) 210°C; 2.17 Kg	ASTM D-1238	8	5	3
Vicat Softening Point (°F/°C)	ASTM D-1525	160/70	180/80	-----
Water Absorption	ASTM D-5170	1.2	1.0	0.8

Dielectric Strength (volts/Mil)	ASTM D-149	360	520	420
Specific Gravity	ASTM D-792	1.2	1.2	1.2
Coefficient of Friction (Kinetic)	ASTM D- 1894	1.5	0.8	0.64
Abrasion Resistance (% loss at 1000 cycles)	ASTM D-1044	0.008	0.035	0.053
Melt Processing Temp. (0°F/0°C)		375-430 / 190-220		
Recommended Sterilization Method		Gamma; E-Beam; ethylene oxide		
Class VI Biocompatibility Test	U.S.P. XXII	Pass	Pass	Pass

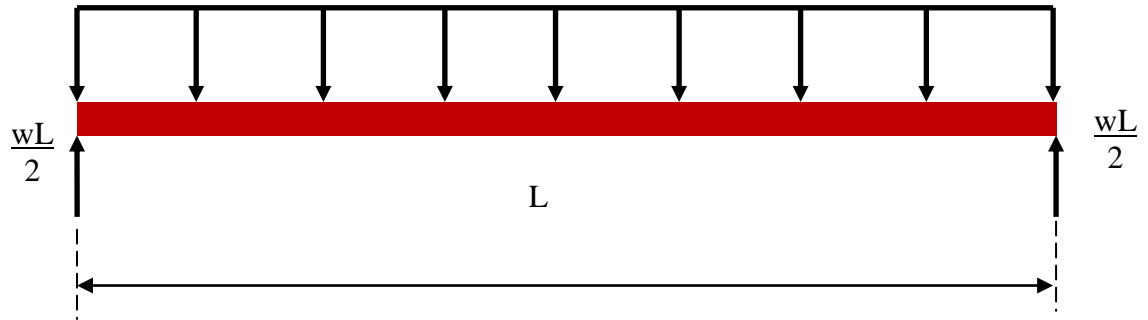
* Specimens conditioned for 7 days at room temperature and 50% R.H.

Physical Properties

Shore Hardness	80A	55D	65D
Appearance	Slightly cloudy	Slightly cloudy	Slightly cloudy
Modulus at 100%	775	1900	5500
Modulus at 300%	600	----	----
Tensile Strength (psi)	6600	7500	9000
Elongation (%)	475	325	250

Information from (http://www.advbiomaterials.com/chronoflex_c_factsheet.html)

Appendix D: hMSC Deflection Derivations



Bending Moment

The differential equation of the deflection curve of the bent beam is:

$$M = EI \frac{d^2y}{dx^2}$$

From the diagram above, the bending moment is:

$$M = \frac{wL}{2}x - \frac{w}{2}x^2$$

E = Young's Modulus
 I = Moment of Inertia
 w = Force on cell per unit length
 L = Length of cell

Setting these two equations equal to each other:

$$EI \frac{d^2y}{dx^2} = \frac{wL}{2}x - \frac{w}{2}x^2$$

Integrate:

$$EI \frac{dy}{dx} = \frac{wL}{4}x^2 - \frac{w}{6}x^3 + C_1$$

Boundary condition 1:

$$\frac{dy}{dx} = 0 \quad @ \quad x = \frac{L}{2} \quad (\text{The slope of the deflection is horizontal at } = \frac{L}{2})$$

Solve for C_1 :

$$0 = \frac{wL}{2} * \frac{L^2}{8} - \frac{w}{2} * \frac{L^3}{24} + C_1$$

$$C_1 = -\frac{wL^3}{24}$$

Plug in C_1 :

$$EI \frac{dy}{dx} = \frac{wL}{4}x^2 - \frac{w}{6}x^3 - \frac{wL^3}{24}$$

Integrate:

$$EIy = \frac{wL}{12}x^3 - \frac{w}{24}x^4 - \frac{wL^3}{24}x + C_2$$

Boundary Condition 2:

$$y = 0 \quad @ \quad x = 0$$

Solve for C_2

$$0 = C_2$$

The maximum deflection occurs at:

$$x = \frac{L}{2}$$

Therefore,

$$EIy_{max} = \frac{wL}{12}x^3 - \frac{w}{24}x^4 - \frac{wL^3}{24}x$$

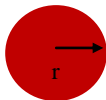
$$EIy_{max} = -\frac{5wL^4}{384}$$

Without regard to the algebraic sign, the maximum deflection at $\frac{L}{2}$ is:

$$\Delta_{max} = \frac{5wL^4}{384EI}$$

CALCULATION FOR THE DEFLECTION OF a hMSC

Cross-Section of a hMSC:



$$r = 5\mu\text{m}$$

$$E = 126 \pm 81 \text{ Pa}$$

$$P = 5 \text{ mmHg} = 266.6 \text{ Pa}$$

Calculation for force on a hMSC ("w")

$$w = \frac{PA}{L}$$

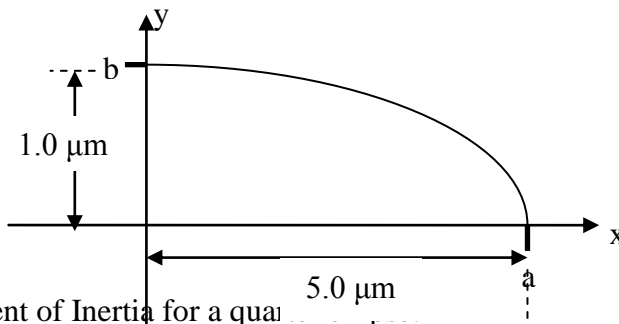
where A=cross-sectional area of a hMSC

$$A = \pi r^2$$

$$w = \frac{(PA\pi r^2)}{L}$$

Calculation for a hMSC's Moment of Inertia ("I")

Since a hMSC has an elliptical shape, the moment of inertia for an ellipse will be used.



Moment of Inertia for a quarter ellipse:

$$I = \frac{\pi a b^3}{16}$$

Since a hMSC will have the shape of a full ellipse, the equation would be:

$$I = \frac{\pi a b^3}{4}$$

$$I = \frac{\pi * 5 * 1^3}{4} \mu\text{m}^4$$

$$I = 3.93 \mu\text{m}^4$$

Maximum deflection of a hMSC

$$\Delta_{max} = \frac{5wL^4}{384EI}$$

Appendix E: hMSC Deflection MatLab Syntax

For L=3.0 micrometers

```
%E=45Pa
E=45*(1/((1*10^6)^2)); %N/micrometer^2
L=3; %micrometer
a=5; %micrometer
b=1; %micrometer
w=(266.6*(1/((1*10^6)^2))*25*pi)/3; %N/micrometer
I=(pi*a*(b^3))/4
  %I=3.927 micrometers^4
d=(5/384)*((w*(L^4))/(E*I))
  %d = 41.6563 micrometers
```

```
%E=126Pa
E=126*(1/((1*10^6)^2)); %N/micrometer^2
L=3; %micrometer
a=5; %micrometer
b=1; %micrometer
w=(266.6*(1/((1*10^6)^2))*25*pi)/3; %N/micrometer
I=(pi*a*(b^3))/4;
  %I=3.927 micrometers^4
d=(5/384)*((w*(L^4))/(E*I))
  %d = 14.88 micrometers
```

```
%E=207Pa
E=207*(1/((1*10^6)^2)); %N/micrometer^2
L=3; %micrometer
a=5; %micrometer
b=1; %micrometer
w=(266.6*(1/((1*10^6)^2))*25*pi)/3; %N/micrometer
I=(pi*a*(b^3))/4;
  %I=3.927 micrometers^4
d=(5/384)*((w*(L^4))/(E*I))
  %d = 9.0557 micrometers
```

For L=2.5 micrometers

```
%E=45Pa
E=45*(1/((1*10^6)^2)); %N/micrometer^2
L=2.5; %micrometer
a=5; %micrometer
b=1; %micrometer
w=(266.6*(1/((1*10^6)^2))*25*pi)/2.5; %N/micrometer
I=(pi*a*(b^3))/4
  %I=3.927 micrometers^4
d=(5/384)*(w*(L^4))/(E*I)
  %d = 24.11 micrometers
```

```
%E=126Pa
E=126*(1/((1*10^6)^2)); %N/micrometer^2
L=2.5; %micrometer
a=5; %micrometer
b=1; %micrometer
w=(266.6*(1/((1*10^6)^2))*25*pi)/2.5; %N/micrometer
I=(pi*a*(b^3))/4;
  %I=3.927 micrometers^4
d=(5/384)*(w*(L^4))/(E*I)
  %d = 8.61 micrometers
```

```
%E=207Pa
E=207*(1/((1*10^6)^2)); %N/micrometer^2
L=2.5; %micrometer
a=5; %micrometer
b=1; %micrometer
w=(266.6*(1/((1*10^6)^2))*25*pi)/2.5; %N/micrometer
I=(pi*a*(b^3))/4;
  %I=3.927 micrometers^4
d=(5/384)*(w*(L^4))/(E*I)
  %d = 5.24 micrometers
```

For L=2.0 micrometers

```
%E=45Pa
E=45*(1/((1*10^6)^2)); %N/micrometer^2
L=2; %micrometer
a=5; %micrometer
b=1; %micrometer
w=(266.6*(1/((1*10^6)^2))*25*pi)/2; %N/micrometer
I=(pi*a*(b^3))/4
  %I=3.927 micrometers^4
d=(5/384)*(w*(L^4))/(E*I)
  %d = 12.34 micrometers
```

```
%E=126Pa
E=126*(1/((1*10^6)^2)); %N/micrometer^2
L=2; %micrometer
a=5; %micrometer
b=1; %micrometer
w=(266.6*(1/((1*10^6)^2))*25*pi)/2; %N/micrometer
I=(pi*a*(b^3))/4;
  %I=3.927 micrometers^4
d=(5/384)*(w*(L^4))/(E*I)
  %d = 4.41 micrometers
```

```
%E=207Pa
E=207*(1/((1*10^6)^2)); %N/micrometer^2
L=2; %micrometer
a=5; %micrometer
b=1; %micrometer
w=(266.6*(1/((1*10^6)^2))*25*pi)/2; %N/micrometer
I=(pi*a*(b^3))/4;
  %I=3.927 micrometers^4
d=(5/384)*(w*(L^4))/(E*I)
  %d = 2.68 micrometers
```

For $L=1.5$ micrometers

```
%E=45Pa
E=45*(1/((1*10^6)^2)); %N/micrometer^2
L=1.5; %micrometer
a=5; %micrometer
b=1; %micrometer
w=(266.6*(1/((1*10^6)^2))*25*pi)/1.5; %N/micrometer
I=(pi*a*(b^3))/4
  %I=3.927 micrometers^4
d=(5/384)*(w*(L^4))/(E*I)
  %d = 5.21 micrometers
```

```
%E=126Pa
E=126*(1/((1*10^6)^2)); %N/micrometer^2
L=1.5; %micrometer
a=5; %micrometer
b=1; %micrometer
w=(266.6*(1/((1*10^6)^2))*25*pi)/1.5; %N/micrometer
I=(pi*a*(b^3))/4;
  %I=3.927 micrometers^4
d=(5/384)*(w*(L^4))/(E*I)
  %d = 1.86 micrometers
```

```
%E=207Pa
E=207*(1/((1*10^6)^2)); %N/micrometer^2
L=1.5; %micrometer
a=5; %micrometer
b=1; %micrometer
w=(266.6*(1/((1*10^6)^2))*25*pi)/1.5; %N/micrometer
I=(pi*a*(b^3))/4;
  %I=3.927 micrometers^4
d=(5/384)*(w*(L^4))/(E*I)
  %d = 1.13 micrometers
```

For $L=1.0$ micrometers

```
%E=45Pa
E=45*(1/((1*10^6)^2)); %N/micrometer^2
L=1; %micrometer
a=5; %micrometer
b=1; %micrometer
w=(266.6*(1/((1*10^6)^2))*25*pi)/1; %N/micrometer
I=(pi*a*(b^3))/4
  %I=3.927 micrometers^4
d=(5/384)*(w*(L^4))/(E*I)
  %d = 1.54 micrometers
```

```
%E=126Pa
E=126*(1/((1*10^6)^2)); %N/micrometer^2
L=1; %micrometer
a=5; %micrometer
b=1; %micrometer
w=(266.6*(1/((1*10^6)^2))*25*pi)/1; %N/micrometer
I=(pi*a*(b^3))/4;
  %I=3.927 micrometers^4
d=(5/384)*(w*(L^4))/(E*I)
  %d = 0.55 micrometers
```

```
%E=207Pa
E=207*(1/((1*10^6)^2)); %N/micrometer^2
L=1; %micrometer
a=5; %micrometer
b=1; %micrometer
w=(266.6*(1/((1*10^6)^2))*25*pi)/1; %N/micrometer
I=(pi*a*(b^3))/4;
  %I=3.927 micrometers^4
d=(5/384)*(w*(L^4))/(E*I)
  %d = 0.33 micrometers
```

For $L=0.4$ micrometers

```
%E=45Pa
E=45*(1/((1*10^6)^2)); %N/micrometer^2
L=0.4; %micrometer
a=5; %micrometer
b=1; %micrometer
w=(266.6*(1/((1*10^6)^2))*25*pi)/0.4; %N/micrometer
I=(pi*a*(b^3))/4
  %I=3.927 micrometers^4
d=(5/384)*(w*(L^4))/(E*I)
  %d = 0.0987 micrometers
```

```
%E=126Pa
E=126*(1/((1*10^6)^2)); %N/micrometer^2
L=0.4; %micrometer
a=5; %micrometer
b=1; %micrometer
w=(266.6*(1/((1*10^6)^2))*25*pi)/0.4; %N/micrometer
I=(pi*a*(b^3))/4;
  %I=3.927 micrometers^4
d=(5/384)*(w*(L^4))/(E*I)
  %d = 0.0353 micrometers
```

```
%E=207Pa
E=207*(1/((1*10^6)^2)); %N/micrometer^2
L=0.4; %micrometer
a=5; %micrometer
b=1; %micrometer
w=(266.6*(1/((1*10^6)^2))*25*pi)/0.4; %N/micrometer
I=(pi*a*(b^3))/4;
  %I=3.927 micrometers^4
d=(5/384)*(w*(L^4))/(E*I)
  %d = 0.0215 micrometers
```

Appendix F: Tables of all Deflection Calculations

Length between Fibers = 3.0 μm		
Pressure (Pa)	E (Pa)	d (μm)
133.3	45	20.78
	126	7.42
	207	4.52
266.6	45	41.66
	126	14.88
	207	9.06
666.6	45	104.16
	126	37.2
	207	22.64
799.9	45	124.98
	126	44.64
	207	27.17

Length between Fibers = 2.5 μm		
Pressure (Pa)	E (Pa)	d (μm)
133.3	45	12.03
	126	4.3
	207	2.61
266.6	45	24.11
	126	8.61
	207	5.24
666.6	45	60.28
	126	21.53
	207	13.1
799.9	45	72.33
	126	25.83
	207	15.72

Length between Fibers = 2.0 μm		
Pressure (Pa)	E (Pa)	d (μm)
133.3	45	6.16
	126	2.2
	207	1.34
266.6	45	12.34
	126	4.41
	207	2.68
666.6	45	30.86
	126	11.02
	207	6.71
799.9	45	37.03
	126	13.23
	207	8.05

Length between Fibers = 1.5 μm		
Pressure (Pa)	E (Pa)	d (μm)
133.3	45	2.6
	126	0.93
	207	0.56
266.6	45	5.21
	126	1.86
	207	1.13
666.6	45	13.02
	126	4.65
	207	2.83
799.9	45	15.62
	126	5.58
	207	3.4

Length between Fibers = 1.0 μm		
Pressure (Pa)	E (Pa)	d (μm)
133.3	45	0.77
	126	0.27
	207	0.17
266.6	45	1.54
	126	0.55
	207	0.33
666.6	45	3.86
	126	1.38
	207	0.84
799.9	45	4.63
	126	1.65
	207	1.01

Length between Fibers = 0.4 μm		
Pressure (Pa)	E (Pa)	d (μm)
133.3	45	0.0493
	126	0.0176
	207	0.0107
266.6	45	0.0987
	126	0.0353
	207	0.0215
666.6	45	0.2469
	126	0.0882
	207	0.0537
799.9	45	0.2963
	126	0.1058
	207	0.0644

Bibliography

AdvanSource Biomaterials. (2008). *ChronoFlex[®] C: Biodurable medical grade polyurethane*.

Retrieved 6 Mar., 2009, from http://www.advbiomaterials.com/chronoflex_c_factsheet.html

Alliance for the Polyurethanes Industry. (2001). The use of polyurethanes in medical device applications. *Technical Report*,

American Heart Association, I. (2008). *Atrial fibrillation*. Retrieved October 16, 2008, from

<http://www.americanheart.org/presenter.jhtml?identifier=4451>

Boretos, Tohn W., and William S. Pierce. (1967). Segmented polyurethane: A new elastomer for biomedical applications *Science, New Series*, 158, 1481-1482.

Bronzino, J. D. (2006). *The biomedical engineering handbook, third edition*

Center for disease control website. <http://www.cdc.gov/heartdisease/>

Doble, Mukesh, Nilesh Makadia, Sreejs Pavithran, and R Suresh Kumar. (2008). Analysis of explanted ePTFE cardiovascular grafts (modified BT shunt). *Biomadical Materials*, 3, 9.

Elhendy, Abdou , MD, PhD, FACC, FAHA, Stein, Kenneth M. , M.D., FACC & Mittal, Suneet , M.D., FACC. (2008). *Pacemaker*. Retrieved September 10, 2008

<http://yourtotalhealth.ivillage.com/pacemaker.html?pageNum=12>

Forte, G., Minieri, M., Cossa, P., Antenucci, D., Sala, M., Gnocchi, V., et al. (2005). Hepatocyte growth factor effects on mesenchymal stem cells: Proliferation, migration, and differentiation. *Stem Cells Express*, 24, 23-23-33.

- Fox, S. I. (2008). *Human physiology* (10th ed.). New York: McGraw-Hill.
- Geddes, L. A., & Tacker, J., W.A. (1980). *Electrical defibrillation* CRC Press, Inc.
- Geiger G. (1991). Deterioration of PTFE-prosthesis wall. ASEM study. *Journal of Cardiovascular Surgery*, 32, 660-663.
- Ghista, D. N., Mirsky, I., & Sandler, H. (1974). *Cardiac mechanics: Physiological, clinical, and mathematical considerations* John Wiley & Sons, Inc.
- Ghista, D. N., & Yin-Kwee Ng, E. (2007). *Cardiac perfusion and pumping engineering* World Scientific Publishing Co. Pte. Ltd.
- Giudiceandrea A, Seifalian AM, Krijgsman B, Hamilton G. (1998). Effect of prolonged pulsatile shear stress in vitro on endothelial cell seeded PTFE and compliant polyurethane vascular grafts. *Eur J Vasc Endovasc Surg*, 15, 147-154.
- Grossman, W., Jones, D., & McLaurin, L. P. (1975). Wall stress and patterns of hypertrophy in the human left ventricle. *The Journal of Clinical Investigation*, 56, 56-64.
- Heineman, F. W., & Grayson, J. (1985). Transmural distribution of intramyocardial pressure measured by micropipette technique. *American Journal of Physiology of Heart and Circulatory Physiology*, 249(6), 1216-1223.
- Homan Van Der Heide, J.N., M.D., Nieveen, J., M.D., Thalen, H. J. T., M.D., & Van Den Berg, JW., D.S.C. (1970). *The artificial cardiac pacemaker* Royal VanGorcum Ltd.
- Ilana Cohen. (2005). Biomaterials in cardiology. *InspiredMD Corporation*,

- Isaka, Mitsuhiro, Toshiya Nishibe, Yasuhiro Okuda, Masaru Saito, Takahiro Seno, Kazuto Yamashita, Yasuharu Izumisawa, Tadao Kotani, and Keishu Yasuda. (2006). Experimental study on stability of a high-porosity expanded polytetrafluoroethylene graft in dogs. *Annals of Thoracic Cardiovascular Surgery*, 12, 37-41.
- Jia, Wenji, Mark W. Beatty, Richard A. Reinhardt, Thomas M. Petro, Donald M. Cohen, Constance R. Maze, E. A. Strom, and Melvin Hoffman. (1999). Nickel release from orthodontic arch wires and cellular immune response to various nickel concentrations. *Journal of Applied Biomaterials*, 48, 488-495.
- KacKay, T. G., Wheatley, D. J., Bernacca, G. M., Fisher, A. C. and Hindle, C. S. (1996). New polyurethane heart valve prosthesis: Design, manufacture and evaluation. *Biomaterials*, 17, 1857.
- Kajiwara, Hirokazu, Toshiyuki Hamada, Yukio Ichikawa, Masanori Ishi, and Ichiya Yamazaki. (2004). Experience with expanded polytetrafluoroethylene (ePTFE gore-tex) surgical membrane for coronary artery grafting: Does ePTFE surgical membrane predispose to postoperative mediastinitis? *Artificial Organs*, 28, 840-845.
- Katz, A. M., M.D. (1977). *Physiology of the heart* Raven Press Books, Ltd.
- Klabunde, Richard E. , Ph.D. (2008). *Cardiovascular physiology concepts*. Retrieved September 14, 2008 <http://www.cvphysiology.com/Arrhythmias/A004.htm>
- Levy, M. N., & Pappano, A. (2007). *Cardiovascular physiology* Mosby, Inc.

M Radisic, H Park, H Shing, T Consi, FJ Schoen, R. (2004). Functional assembly of engineered myocardium by electrical stimulation of cardiac myocytes cultured on scaffolds.

Proceedings of the National Academy of Sciences of the United States of America, 101(52), 18129-18134.

Ma, Peter X., and Jennifer Elisseeff. (2005). *Scaffolding in tissue engineering*. New York: C R C P LLC.

Mackay, T. G., Wheatley, D. J., Bernacca, G. M., Fisher, A. C., & Hindle, C. S. (1996). New polyurethane heart valve prosthesis: Design, manufacture and evaluation. *Biomaterials*, 17(19), 1857-1863. doi:DOI: 10.1016/0142-9612(95)00242-1

Martinez-Martinez L., Pascual A. and Perez, E. J. (1990). Effect of three plastic catheters on survival and growth of pseudomonas aeruginosa *J. Hospital Infec*, 16, 311.

Myers, G. H., & Parsonnet, V. (1969). *Engineering in the heart and blood vessels* John Wiley & Sons, Inc.

Pedicini, A., & Farris, R. J. (2003). Mechanical behavior of electrospun polyurethane. *Polymer*, 44, 6857-6862.

Pelton, A. R., D. Stockel, and T. W. Duerig. (2000). Medical uses of nitinol. *Materials Science Forums*, 327, 63-70.

Peter X, M., & Elisseeff, J. (2005). *Scaffolding in tissue engineering*

- Potapova, I., Plotnikov, A., Lu, Z., Danilo, P., Jr, Valiunas, V., Qu, J., et al. (2004). Human mesenchymal stem cells as a gene delivery system to create cardiac pacemakers. *Circulation Research*, 94(7), 952-959. doi:10.1161/01.RES.0000123827.60210.72
- Ritter, E., MD, Perry, A., MD, Yu, Jack, MD, DDS., Wang, Thomas, MD, PhD, Tang, L., MD, & Bieberich, E., PhD. (2008). Breast cancer cell-derived fibroblast growth factor 2 and vascular endothelial growth factor are chemoattractants for bone marrow stromal stem cells. *Annals of Surgery*, 247(2), 310.
- Rosen, M., R., Brink, P., R., Cohen, I., S., & Robinson, R., B. (2007). Biological Pacemakers based on I_f . *Medical and Biological Engineering and Computing*, 24(2), 157-166.
- Rosen, M. R., Brink, P. R., Cohen, I. S., & Robinson, R. B. (2004). Genes, stem cells and biological pacemakers. *Cardiovascular Research*, 64(1), 12-23.
doi:10.1016/j.cardiores.2004.05.012
- Ryhanen, J., M. Kallioinen, J. Tuukkanen, J. Junila, E. Niemela, P. Sandvik, and W. Serlo. (1998). In vivo biocompatibility evaluation of nickel-titanium shape memory metal alloy: Muscle and perineural tissue responses and capsule membrane thickness. *Journal of Biomedical Materials Research*, 41, 481-488.
- Sarkar, S., Salacinski, H. J., Hamilton, G., & Seifalian, A. M. (2006). The mechanical properties of infrainguinal vascular bypass grafts: Their role in influencing patency. *European Journal of Vascular and Endovascular Surgery*, 31(6), 627-636. doi:DOI: 10.1016/j.ejvs.2006.01.006

- Sherwood, L. (2003). *Human physiology: From cells to systems* Brooks Cole.
- Sherwood, L. (2004). *Human physiology: From cells to systems* (Fifth ed.) Brookscole.
- Tan, S., Pan, W., Ma, G., Cai, N., Leong, K., & Liao, K. (2008). Viscoelastic behaviour of human mesenchymal stem cells. *BME Cell Biology*, 9, 1-7.
- Tastan, I., Schreckenber, R., Mufti, S., Abdallah, Y., Piper, H. M., & Schluter, K. (2009). Parathyroid hormone improves contractile performance of adult rat ventricular cardiomyocytes at low concentrations in a non-acute way. *Cardiovascular Research*, , 1-24.
- Trepanier, C., R. Venugopalan, and A. Pelton. (2000). Corrosion resistance and biocompatibility of passivated nitinol. *Shape Memory Implants*, , 35-45.
- Vinoy, Thomas, and Muthu Jayabalan. (2008). A new generation of high flex life polyurethane urea for polymer heart valve - studies on in vivo biocompatibility and biodurability. *Journal of Biomedical Materials Research*, 89A, 192-205.
- Whittaker, David R., and Mark F. Fillinger. (2006). The engineering of endovascular stent technology: A review. *Vascular and Endovascular Surgery*, 40, 85.
- Xiang, Z., Liao, R., Kelly, M. S., Spector, M., Xiang, Z., Liao, R., et al. (2006). Collagena(euro)"GAG scaffolds grafted onto myocardial infarcts in a rat model: A delivery vehicle for mesenchymal stem cells. *Tissue Engineering; Tissue Engineering*, 12(9), 2467-2478.